Hindawi
Shock and Vibration
Volume 2019, Article ID 8156971, 20 pages
https://doi.org/10.1155/2019/8156971

Research Article

Effect of Tooth Profile Modification on Dynamic Tooth Load of Planetary Gear Train

Jiaming Zhou,[1] **Fengyan Yi**,[2] **Xiangyang Xu**,[3,4] **Junbin Lai**,[3,4] **Yanfang Liu**,[3,4] **and Peng Dong**[3,4]

[1]*Department of Vehicle Engineering, School of Mechanical Engineering, Beijing Institute of Technology, Beijing, China*
[2]*Shandong Jiaotong University, Jinan 250357, China*
[3]*Department of Asutomotive Engineering, School of Transportation Science and Engineering, Beihang University, Beijing 100191, China*
[4]*Ningbo Institute of Technology (NIT), Beihang University, Ningbo 315832, China*

Correspondence should be addressed to Junbin Lai; laijunbin5@163.com

Received 15 June 2019; Revised 27 September 2019; Accepted 16 November 2019; Published 10 December 2019

Academic Editor: Mario Terzo

This paper aims at investigating the effects of tooth profile modification (TPM) on the dynamic response of planetary gear train (PGT). A numerical model is carried out to calculate two major excitation sources of PGT, time-varying mesh stiffness (TVMS), and transmission errors (TEs). On this basis, a linear time-varying dynamic model of a PGT considering TVMS, TEs, and TPM is developed. Dynamic deviation factor is further introduced to describe the dynamic response of the PGT. In this paper, TPM is only applied to the external meshes firstly. Effects of TPM parameters, such as amount of TPM, normalized modification angle, and modification curve, on the excitation sources and dynamic response of the PGT are discussed in detail. Subsequently, investigation on the effects of TPM only applied to internal meshes is conducted. Finally, with the aim to obtain the optimal TPM for the minimization of dynamic load of PGT in both external and internal gear meshes, the genetic algorithm (GA) is employed. This research may shed light upon design optimization of PGT with respect to improvement of vibration performance by means of optimized TPM.

1. Introduction

Due to the advantages of large torque-to-weight ratio, compactness, high transmission efficiency, and reduced noise and vibration, planetary gears are widely used in automotive transmission, aerospace, wind turbine, and marine vehicle. Despite of these advantages, noise and vibration still remain a critical issue caused by the manufacturing errors, alignment errors, and tooth deformations. The excitations influencing the noise and vibration of planetary gears can be categorized into two groups: external excitation sources from variation of applied torque and input speed and internal excitation sources from time-varying mesh stiffness (TVMS) and transmission errors (TEs). In these excitations, internal excitations play a decisive role on vibration performance of planetary gear train (PGT). As a result, numerous studies on gear TVMS, TEs, and dynamic behavior of PGT have been carried out.

In previous studies, a finite element (FE) method [1–5] and analytical method [6–17] are widely used to calculate the TVMS and TEs. Obviously, effects of manufacturing errors, assembling errors, and profile deviations can be observed by these two methods. Meanwhile, utilizing the FE method can obtain more accurate results compared with analytical method, but it is excessively time consuming. Therefore, many analytical methods are proposed and its results show great agreements with the FE method. TEs can be classified into no-loaded static transmission error (NLSTE) and loaded static transmission error (LSTE) [3–9]. Taking no account of tooth deflections, the NLSTE represents the deviation between the actual and the theoretical perfect gear

mesh positions. The LSTE relates to the applied torques, TVMS, and NLSTE.

Cornell [10] calculated the mesh stiffness analytically. Yang and Lin [11] employed potential energy principle to calculate the mesh stiffness of gears. And this model was further extended by Wu et al. [12] by taking shear mesh stiffness into consideration. Sainsot et al. [13] proposed an improved tooth fillet-foundation stiffness formula. Using the potential energy principle and considering the tooth fillet-foundation deflection, Charri et al. [14], Chen and Shao [15], and Ma et al. [16] calculated TVMS of cracked gears. Del Rincon et al. [4] obtained the TVMS, LSTE, and load sharing ratio by incorporating the FE method and analytical method. Based on reference [4], Fernández et al. [5] took tooth tip relief and manufacture errors into account to obtain the TVMS and LSTE under different transmitted torques. Xue and Howard [17, 18] found that effects of center distance and carrier arm stiffness on TVMS may not be ignored. Chen and Shao [7] discussed how tooth errors affected the TVMS and LSTE of meshing gear pairs. Ma et al. [8] proposed an improved analytical model to obtain the TVMS and LSTE by taking extended tooth contact into account. TVMS in PGT could be derived by combining the TVMS of one sun-planet meshing pair, one ring-planet meshing pair, and planet phasing [19, 20]. Mainly caused by the change of engaged tooth number during the meshing process, TVMS is unable to be eliminated. The LSTE has a strong correlation with tooth deformation, manufacturing errors, and assembly errors. Besides, tooth profile errors, spacing errors, extended tooth contact, and applied torques influence the TVMS and LSTE deeply.

On the condition of maintaining gear basic geometric parameters invariable, tooth profile modification (TPM) is an effective method to reduce the vibration response in the gear train system. Lin et al. [21] investigated the effects of amount of TPM and modification curve on the dynamic behavior of spur gears. Based on the quasi-static gear tooth contact model, Velex and Maatar [6] observed the best modification parameters for the minimum LSTE of spur and helical gears. Bonori et al. [22] introduced genetic algorithms (GAs) to obtain the optimum modification parameters for minimum fluctuation of the LSTE in spur gears. Considering TVMS, TPM, and contact loss, Liu and Parker [23] proposed a nonlinear analytical model for multimesh gear sets. Dynamic mesh force of individual gear tooth is investigated. Wang and Howard [2] studied the effects of TPM on TVMS, LSTE, loading-sharing ratio, contact stress, and tooth root stress by the FE method. Ghosh and Chakraborty [24] investigated the effects of TPM on dynamic behavior of spur gears and found that optimal TPM depends on operating speeds. Ma et al. [25] developed a profile shifted gear model including TVMS, addendum modifications, and TPM. The results show that optimal profile modification curve depends on the relative peak-peak value of the LSTE. Hu et al. [26] proposed a dynamic model of a high speed gear-rotor-bearing system. Moreover, the effects of TPM on dynamic response of the system are conducted.

Emphasizing on TPM applied in spur gear, previous studies draw a general conclusion that minimum fluctuation of the LSTE results in optimal dynamic response. Nevertheless, having multiple meshing gear pairs and meshing phases, the PGT system is more complicated than the spur gear system. Therefore, it is hard to get the effects of TPM on the dynamic response of PGT. Abousleiman and Velex [27] reported that load distribution on tooth flanks and dynamic tooth loads of PGT get improved after TPM, but detailed information about the selection of modification is not mentioned. Bahk and Parker [28] developed an analytical TPM model for PGT to study effects of TPM on dynamic response of the PGT system. The author concluded that optimal TPM should take the mesh phase between external and internal meshes into account. Furthermore, the TPM scheme corresponding to optimal dynamic response cannot obtain the minimum fluctuation of the LSTE. In this paper, we conduct a detailed investigation of the effects of TPM on internal excitations and dynamic tooth loads of PGT. It should also be mentioned that TVMS and transmission error calculation in this study is based on the model proposed by Chen and Shao [7]. By incorporating the TVMS and transmission error model into the dynamic model of the PGT system, a comprehensive dynamic model including tooth profile modification can be obtained. According to this model, effects of TPM parameters on the dynamic response of the PGT system for external and internal meshes can be studied. The optimal TPM for minimization of dynamic load of the PGT system be further be obtained.

The paper is organized as follows. In Section 1, some previous studies related with TVMS, TEs, and effects of TPM on gear dynamic response are briefly introduced. In Section 2, TPM is introduced for external meshes and internal meshes firstly. Then, an analytical model for calculating TVMS and TEs is developed and a dynamic model of PGT considering the effects of TPM is further established. In Section 3, dynamic deviation factor is defined to quantify the dynamic tooth loads of PGT. The GA is further adopted to optimize the dynamic tooth loads of PGT. In Section 4, effect of TPM applied in external meshes and internal meshes is investigated, respectively. Meanwhile, influence of TPM on TVMS and TEs is also presented. Furthermore, on the purpose of minimizing dynamic tooth loads of PGT, an optimal TPM is obtained by GA. In Section 5, some conclusions are drawn based on the simulation results.

2. Model of PGT considering TPM

Manufacturing errors, assembling errors, and tooth deformations are unavoidable in actual gears. Improper design of tooth profile can cause undesirable noise and vibration in PGT. TPM is an effective method to improve dynamic behavior of PGT. In this section, TPM for external and internal meshes is introduced firstly. Then, based on the relationship between gear tooth errors and internal excitation sources (TVMS and TEs), the corresponding analytical model is proposed. At last, a dynamic model of PGT with TPM is proposed.

2.1. Tooth Profile Modification. TPM can be divided into three types: tooth tip relief, tooth root relief, and the entire profile modification [25]. Tooth tip relief and tooth root relief have the same influence on dynamic behavior of a meshing gear pair [29]. Therefore, modifications of all gears in PGT are assumed to be only applied in tooth tip relief in this study. Figure 1 shows the schematic of tooth tip relief applied in the external and internal gear. The formulation of the tooth tip relief shape is determined by the amount of tip relief C_a and the angle of modification β_a, and can be expressed as follows [25]:

$$\gamma_a = \beta_e - \beta_s;$$
$$C = C_a\left(\frac{\beta - \beta_s}{\gamma_a}\right)^n, \tag{1}$$

where C_a represents the amount of TPM; β_s and β_e denote the angular displacement of the starting point and the ending point of tip relief, respectively; and n is the power exponent and indicates linear tip relief for $n = 1$ and parabolic tip relief for $n = 2$, respectively. The angular displacement β can be written as follows:

$$\beta = \sqrt{\frac{r^2}{r_b^2} - 1} - \theta_b, \tag{2}$$

where r is the radius of instantaneous contact point on the gear; r_b is the base radius of the gear; $\theta_b = \pi/2z + \tan\alpha - \alpha$; and z and α denote the number of teeth and pressure angle, respectively.

In many literatures, the highest point of single-tooth contact (HPSTC) is always selected as the starting modification point in tip relief [7, 25, 26]. To express modification angle better, modification angle corresponding to the starting point located at HPSTC is chosen as reference. We define normalized modification angle as follows:

$$A_n = \frac{\gamma_a}{\gamma_t}, \tag{3}$$

where A_n denotes normalized modification angle and γ_t represents the reference modification angle and can be calculated as $\gamma_t = 2\pi(\varepsilon - 1)/z$ which denotes the contact ratio.

2.2. Calculation of TEs. Due to the manufacturing errors, assembly errors, and applied torque, the actual gear mesh position would deviate from the theoretical, which generates transmission errors and alters mesh stiffness. Figure 2 shows the diagram of a meshing gear pair. The black color of the tooth flank denotes theoretical mesh position, and the blue color of the tooth flank for driving gear represents actual mesh position affected by applied torque and TPM. According to the relationship between the LSTE and gear tooth errors proposed by Chen and Shao [7], the loaded static transmission error (LSTE) can be expressed as follows:

$$\text{LSTE} = E_{d1} + E_{p1} + E_{s1} = E_{d2} + E_{p2} + E_{s2} = E_{d3} + E_{p3} + E_{s3}, \tag{4}$$

and equation (4) could be further written as follows:

$$\text{LSTE} = E_{di} + E_{pi} + E_{si}, \tag{5}$$

where subscript i denotes the ith tooth pair and E_d, E_p, and E_s, respectively, represent the tooth pair deformation, profile error, and separation distance.

Tooth profile error E_p takes positive if material is removed from tooth profile; otherwise, it takes negative, which can be expressed as follows:

$$E_{pi} = E_{pi}^1 + E_{pi}^2, \tag{6}$$

where superscript 1 and 2 denote driving gear and driven gear, respectively. Defined as removing material from tooth surface as intended, TPM can be regarded as a kind of tooth profile error.

Tooth separation distance E_s is defined as the minimum distance of the tooth pair along the line of action in theoretical contact position [30]. Tooth separation distance equals zero if the tooth pair are in contact theoretically.

2.3. Calculation of TVMS. According to the definition of gear tooth profile error E_{pi} and tooth separation distance E_{si} of the ith tooth pair, it can be found that they are independent to the applied torque. Once the gears are mounted on the shafts, E_{pi} and E_{si} are defined. With that, gear tooth error E_r and no-loaded static transmission error (NLSTE) are introduced, which can be expressed as follows:

$$E_{ri} = E_{pi} + E_{si}, \tag{7}$$

$$\text{NLSTE} = \min\left(E_{r1}, E_{r2}, \ldots, E_{rB}\right), \tag{8}$$

where B denotes the total number of contact tooth pairs.

Based on the relative position of tooth pair, Chen and Shao [7] derived the relationship between mesh stiffness and gear tooth errors. According to reference [7], the gear mesh stiffness with gear tooth errors can be expressed as follows:

$$K = \frac{FK_j}{F + \sum_{j=1}^{B} K_j E_{ij}}, \tag{9}$$

where $E_{di} = \max(E_{d1}, E_{d2}, \ldots, E_{dB})$; F is total mesh force; $E_{ij} = E_{rj} - E_{ri}$; and subscript i and j denote the tooth pair number. According to equations (5), (8), and (9), the mesh stiffness could be calculated in a simpler method:

$$\frac{1}{K} = \frac{1}{F}\left(\frac{F + \sum_{j=1}^{B} K_j E_{rj}}{\sum_{j=1}^{B} K_j} - \text{NLSTE}\right). \tag{10}$$

The symbol K_j in equations (9) and (10) is the mesh stiffness of the jth tooth pair, and only when tooth pair contacts work, so that

$$K_j = \begin{cases} K_j, & E_{dj} > 0, \\ 0, & E_{dj} \le 0. \end{cases} \tag{11}$$

Both external mesh and internal mesh are included in planetary gears. Since ring gear is fixed by connecting to the gearbox in many cases, the deformation of fillet-foundation

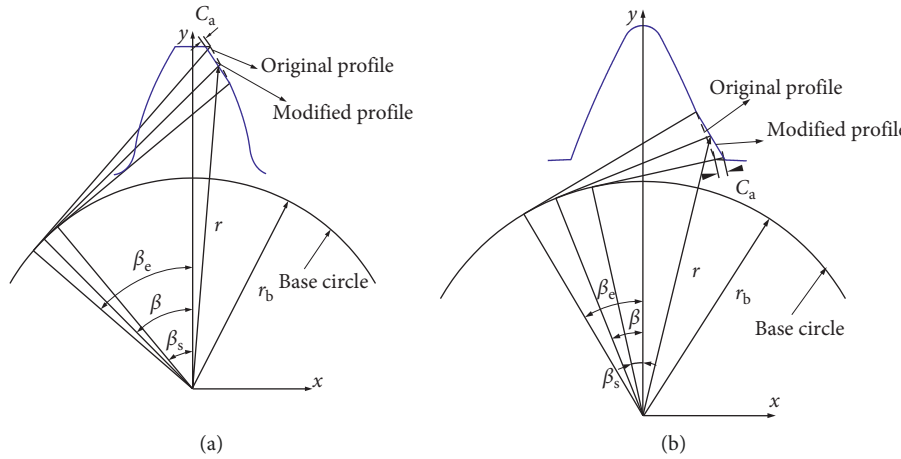

Figure 1: The schematic of tooth tip relief: (a) external gear and (b) internal gear.

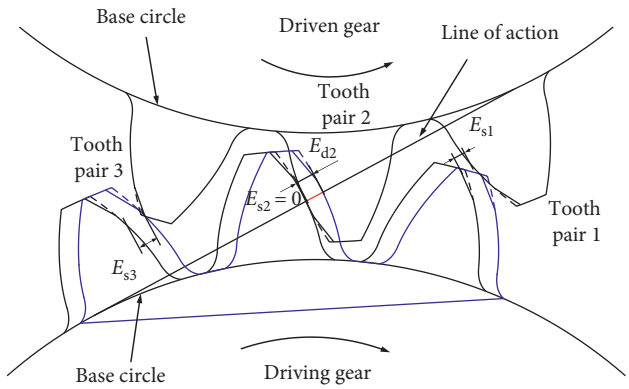

Figure 2: Diagram of a meshing gear pair.

of ring gear is neglected in this paper. Mesh stiffness of a single-tooth pair could be written as follows [15]:

$$\frac{1}{K_j} = \begin{cases} \dfrac{1}{K_h} + \dfrac{1}{K_{\text{ext}}^1} + \dfrac{1}{K_{\text{ext}}^2}, & \text{external mesh,} \\ \dfrac{1}{K_h} + \dfrac{1}{K_{\text{ext}}} + \dfrac{1}{K_{\text{int}}}, & \text{internal mesh,} \end{cases} \tag{12}$$

where K_h denotes the stiffness with respect to Hertzian contact deformation between the gear teeth; the superscripts 1 and 2 denote the driving gear and driven gear in the external mesh, respectively; K_{ext} and K_{int} represent, respectively, the stiffness of the external and internal gear tooth, and can be calculated as follows:

$$\begin{aligned} \frac{1}{K_{\text{ext}}} &= \frac{1}{K_{\text{b}}} + \frac{1}{K_{\text{s}}} + \frac{1}{K_{\text{a}}} + \frac{1}{K_{\text{f}}}, \\ \frac{1}{K_{\text{int}}} &= \frac{1}{K_{\text{b}}} + \frac{1}{K_{\text{s}}} + \frac{1}{K_{\text{a}}}, \end{aligned} \tag{13}$$

where K_{b}, K_{s}, K_{a}, and K_{f} represent the stiffness due to the effect of tooth bending, shear, and axial compressive deformation and fillet-foundation deformation, respectively. All these stiffness could be calculated by the potential energy method, and more detailed information can be obtained in reference [15].

2.4. Modeling of PGT. The planetary gear dynamic model investigated in this paper is a one-stage PGT as shown in Figure 3 [31]. It contains a sun gear (s), a carrier (c), a ring gear (r), and N planets (p). In this paper, deflections of the carrier and the gear body are ignored. All gears are regarded as rigid bodies supported with compliant bearings and connected with each other by linear springs acting on the lines of action. Each component is assumed to own three degrees of freedom (two translations and one rotation). The rotational coordinate can be defined as $u_j = r_j\theta_j$ (j = s, r, c, p1, . . ., pN), where θ_j is the angular displacement. The symbol r_j represents the base radius for gears and the radius of the circle passing through the planet centers for carrier. The translational coordinates for the sun gear, the ring gear, and the carrier are x_j, y_j (j = s, r, c). The coordinate x_j (j = s, r, c) is directed towards the equilibrium position of planet #1. The planet translations x_{pn} and y_{pn} ($n = 1, \ldots, N$), which represent, respectively, the radial and tangential deflections of planet #n [32] are measured with respect to a rotating reference frame fixed to the carrier with the origin O. It is supposed that the geometrical parameter and profile shape of all planet gears are identical and the effect of dampness and gravity are neglected. The excitations in the planetary system are contributed by (i) periodic TVMS of sun-planet #n gear pair (s − pn) $k_{\text{spn}}(t)$ and ring-planet #n gear pair (r − pn) $k_{\text{rpn}}(t)$ and (ii) periodic displacement excitations $\text{NLSTE}_{\text{spn}}$ and $\text{NLSTE}_{\text{rpn}}$.

The relative gear mesh displacement along the line of action can be given as follows:

$$\begin{aligned} p_{\text{jpn}}(t) = {} & y_j(t)\cos\psi_{\text{jpn}} - x_j(t)\sin\psi_{\text{jpn}} - y_{\text{pn}}(t)\cos\alpha_j \\ & - \delta_j x_{\text{pn}}(t)\sin\alpha_j + u_j(t) + \delta_j u_{\text{pn}}(t) - \text{NLSTE}_{\text{jpn}}(t), \end{aligned} \tag{14}$$

where $\psi_{\text{jpn}} = \varphi_n - \delta_j\alpha_j$ and the angle φ_n is the circumferential planet location of planet #n measured relative to the rotating frame with $\varphi_1 = 0$. The symbol $\delta_j = 1$ stands for j = s (external gear mesh) and $\delta_j = -1$ for j = r (internal gear mesh), and α_j denotes the pressure angle of the gears. The dynamic mesh of the gear pair could be further defined as follows:

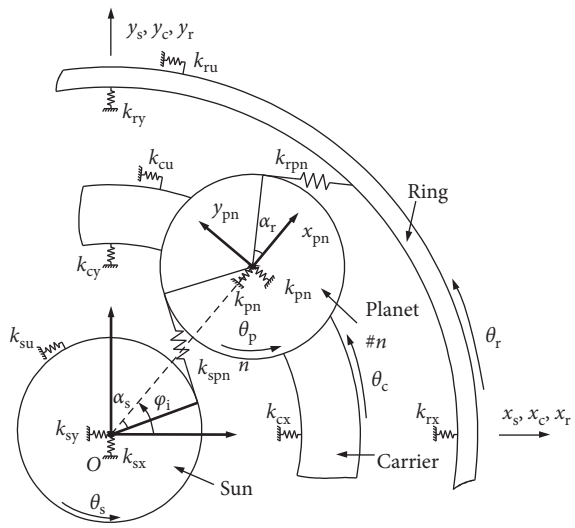

FIGURE 3: The dynamic model of planetary gear train.

$$F_{\mathrm{jpn}}(t) = k_{\mathrm{jpn}}(t)\, p_{\mathrm{jpn}}(t). \tag{15}$$

The total number of degrees of freedom is $3N + 9$ for the planetary system, and the global equation of motion of the system can be written in a matrix form as follows [32]

$$\mathbf{M}\ddot{\mathbf{X}}(t) + \Omega_c \mathbf{G}\dot{\mathbf{X}}(t) + \left[\mathbf{K}_b + \mathbf{K}_m(t) - \Omega_c^2 \mathbf{K}_\Omega\right]\mathbf{X}(t) = \mathbf{T} + \mathbf{F}(t), \tag{16a}$$

$$\mathrm{X} = \left[x_c, y_c, u_c, x_r, y_r, u_r, x_s, y_s, u_s, x_{p1}, y_{p1}, u_{p1}, \ldots, x_{pN}, y_{pN}, u_{pN}\right]^T, \tag{16b}$$

where $\mathbf{M}$ is mass matrix. $\mathbf{X}$ denotes the vector of the degrees of freedom and superscript T represents transpose of the vector. Ω_c is the angular speed of carrier. $\mathbf{K}_b$ and $\mathbf{K}_m(t)$ denote the bearing stiffness matrix and gear mesh stiffness matrix, respectively. $\mathbf{G}$ and $\mathbf{K}_\Omega$ stand for gyroscopic matrix and centripetal matrix, respectively. $\mathbf{T}$ denotes the external torques applied to the planetary system. $\mathbf{F}(t)$ is the excitation force induced by the NLSTE and can be expressed as

$$\mathbf{F}(t) = \left[\mathbf{0}, \mathbf{F}_r(t), \mathbf{F}_s(t), \mathbf{F}_1(t), \ldots, \mathbf{F}_N(t)\right]^T, \tag{17a}$$

$$\mathbf{F}_r(t) = \sum_{n=1}^{N} k_{\mathrm{rpn}}(t)\mathrm{NLSTE}_{\mathrm{rpn}}(t)\left[-\sin\psi_{\mathrm{rpn}}, \cos\psi_{\mathrm{rpn}}, 1\right]^T, \tag{17b}$$

$$\mathbf{F}_s(t) = \sum_{n=1}^{N} k_{\mathrm{spn}}(t)\mathrm{NLSTE}_{\mathrm{spn}}(t)\left[-\sin\psi_{\mathrm{spn}}, \cos\psi_{\mathrm{spn}}, 1\right]^T, \tag{17c}$$

$$\mathbf{F}_n(t) = \sum_{j}^{s,r} k_{\mathrm{jpn}}(t)\mathrm{NLSTE}_{\mathrm{jpn}}(t)\left[-\delta_j \sin\alpha_j, -\cos\alpha_j, \delta_j\right]. \tag{17d}$$

By introducing TVMS and NLSTE into the motion equation of planetary system (equations (16a), (16b), and (17a)–(17d)), the dynamic vibration response of the system can be achieved by the Newmark-β method. Once the planetary design parameters are determined and the external torque remains constant, two main excitations of the system TVMS and NLSTE can be defined. Based on the theory discussed above, it can be observed that TPM has a great effect on these excitations. As a result, TPM is an effective approach to reduce the vibration behavior of the planetary system.

2.5. Model Validation. Inalpolat and Kahraman [33] have put an effort in describing the vibration signal of an accelerometer fixed to the ring gear which is held stationary on the gearbox through bolts and pins. Figure 4 shows the schematic of a 4-planet PGT with an accelerometer mounted on the ring gear. For a complete revolution of the planet carrier, it is assumed that individual influence of planet $\#i$ on the accelerometer lasts for $2\pi/(\Omega_c N)$. Combining Hanning window functions with Heaviside unit functions, the acceleration signal on the ring gear outer surface can be expressed as follows:

$$a(t) = \sum_{n=1}^{N} c w_n(t) F_n(t), \tag{18a}$$

$$A(\omega) = \int_{-\infty}^{\infty} \left| a(t) e^{-i\omega t} \right| \mathrm{d}t, \tag{18b}$$

where $a(t)$ is the acceleration propagated to the accelerometer and $A(\omega)$ represents the corresponding frequency spectrum. c stands for a constant related to dynamic mesh force, $w_n(t)$ for weighing function, and $F_i(t)$ for the total dynamic mesh force at the ring-planet $\#i$ interface. More detailed information about equations (18a) and (18b) can be found in reference [33].

Figure 5 shows the dimensionless acceleration spectra focused on two planetary gear set types as measured and simulated by Inalpolat and Kahraman [33] along with the results provided by the proposed model in this section. The peak positions and their relative amplitudes are in very good agreement. The peak positions are symmetrical about the mesh order $H_m(H_m = z_r)$ and appears at even integer orders. It is indicated that the proposed model is valid for investigating the dynamic response of the PGT.

3. Evaluation and Optimization of PGT

3.1. Dynamic Deviation Factor. Dynamic deviation factor, an effective method to quantify the dynamic tooth loads of PGT, is suggested by Abousleiman and Velex [27, 34] that can be written as follows:

$$S^{\mathrm{ext}} = \frac{1}{N}\sum_{n=1}^{N}\sqrt{\frac{1}{N_{\mathrm{calc}}}\sum_{k=1}^{N_{\mathrm{calc}}}\left(F_{\mathrm{nk}}^{\mathrm{ext}} - F_{\mathrm{stat}}^{\mathrm{ext}}\right)^2}, \tag{19a}$$

$$S^{\mathrm{int}} = \frac{1}{N}\sum_{n=1}^{N}\sqrt{\frac{1}{N_{\mathrm{calc}}}\sum_{k=1}^{N_{\mathrm{calc}}}\left(F_{\mathrm{nk}}^{\mathrm{int}} - F_{\mathrm{stat}}^{\mathrm{int}}\right)^2}, \tag{19b}$$

where S^{ext} and S^{int} denote external meshes (sun-planet) and internal meshes (ring-planet) dynamic deviation factors,

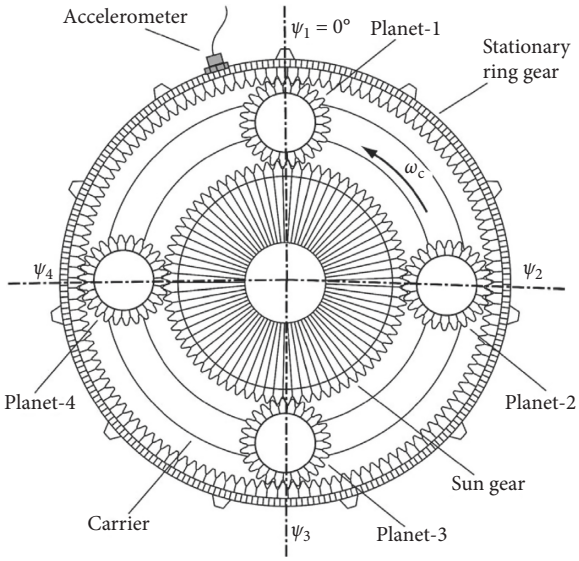

Figure 4: A schematic of a 4-planet PGT with an accelerometer mounted on the ring gear [33].

respectively; N_{calc} represents number of time increments for averaging S^{ext} and S^{int}; F_{nk}^{ext} and F_{nk}^{int} stand for instantaneous mesh force on sun-planet #n and ring-planet #n meshes, respectively; and F_{stat}^{ext} and F_{stat}^{int} are static mesh force over one mesh cycle on external and internal meshes, respectively.

It is suggested that reduced dynamic deviation factor can improve the dynamic behavior of PGT and reduce the vibration and noise [27]. In order to quantify the effect of TPM on the dynamic tooth loads of PGT, we define relative dynamic deviation factor as follows:

$$R_{s,ext} = \frac{S_n^{ext} - S_m^{ext}}{S_n^{ext}} \times 100\%, \tag{20a}$$

$$R_{s,int} = \frac{S_n^{int} - S_m^{int}}{S_n^{int}} \times 100\%, \tag{20b}$$

where R_s denotes relative dynamic deviation factor. Subscripts ext and int refer to external meshes and internal meshes, respectively. S_m and S_n represent dynamic deviation factor with and without TPM, respectively. If the value of the relative dynamic deviation factor is positive, the corresponding dynamic tooth loads get improved and vice versa.

3.2. Optimization of TPM. The primary goal of TPM is to reduce the vibration and noise of PGT, so that TPM should improve the dynamic tooth loads for both external and internal meshes. Since dynamic deviation factor relates with instantaneous mesh force, which has great dependence on TPM parameters, optimization selection of TPM is a multiple parameter problem. GA has been confirmed as an efficient method to handle multiple parameter optimization problem in the gear train system [22, 35].

GA is a stochastic optimization algorithm that mimics natural selection [36]. Figure 6(a) shows the flow chart of the GA computational model.

In this paper, we assume that amount of TPM and normalized modification angle is identical for sun gear and all the planet gears in external meshes. And this assumption also applies to internal meshes. As a result, there exist four TPM parameters forming an individual X, which can be written as follows:

$$X = [C_{ext}; A_{ext}; C_{int}; A_{int}], \tag{21}$$

where C denotes the amount of TPM, A represents normalized modification angle, subscripts ext and int refer to external meshes and internal meshes, respectively. Figure 6(b) shows the encoding of an individual. Each individual comprises four TPM parameters, and each TPM parameter is transformed into a string of alternating 0s and 1s by binary encoding.

Fitness is a function related with the relative dynamic deviation factor, since purpose of TPM aims to improve the dynamic tooth loads of PGT. Previous literatures conduct the dynamic deviation factor in a wide operating speed range to investigate the dynamic response of PGT [27, 34]. Optimal TPM implies that dynamic tooth loads in external and internal meshes decrease over a wide operating range. However, it is unrealistic considering vibration response over the entire speed range for fitness function. In order to evaluate the effectiveness of TPM, two operating speeds, which correspond to the first two peak amplitude of the dynamic deviation factor without TPM, are, respectively, selected in external meshes and internal meshes. Therefore, we define the fitness function as follows:

$$F(X) = \left(R_{s,ext}^1 + R_{s,ext}^2 + R_{s,int}^1 + R_{s,int}^2\right) \Theta \left(\frac{R_{s,ext}^1}{\left|R_{s,ext}^1\right|} + \frac{R_{s,ext}^2}{\left|R_{s,ext}^2\right|} + \frac{R_{s,int}^1}{\left|R_{s,int}^1\right|} + \frac{R_{s,int}^2}{\left|R_{s,int}^2\right|} - 3 \right), \tag{22}$$

where superscripts 1 and 2 denote the operating speed at the first and second dynamic deviation factor peak amplitude without TPM. The symbol Θ is defined as follows:

$$\Theta(R_s) = \begin{cases} 1, & R_s \geq 0, \\ 0, & R_s < 0. \end{cases} \tag{23}$$

The presented GA improves the solution by means of a certain number of iterations on a population with some individuals. Each iteration has three steps: selection, crossover, and mutation. Figure 6(c) shows the principle of crossover, and Figure 6(d) shows the principle of mutation. More details about the GA can be found in Ref. [32].

4. Results and Discussions

In what follows, a single spur PGT with three equally spaced planets is investigated, and the basic parameters are listed in Table 1. The ring gear is fixed and power flows from the sun input to the carrier output. No floating members are allowed. Effects of TPM parameters on TVMS and TEs for external meshes are discussed, and the dynamic tooth loads

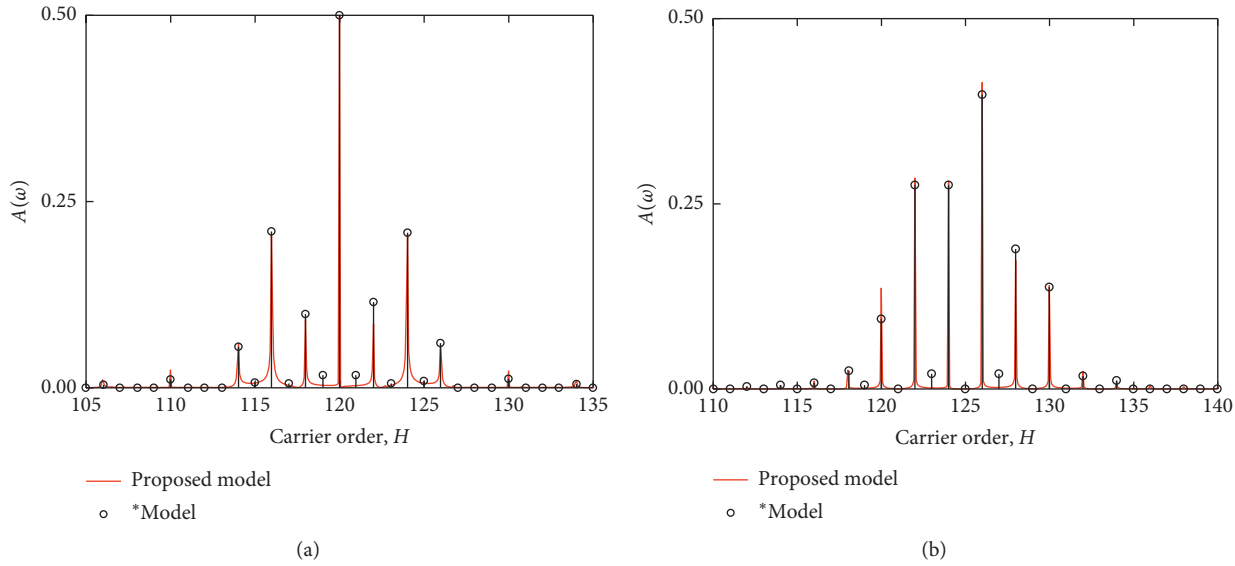

Figure 5: Acceleration spectra on the ring gear for (a) $N = 4$, $z_r = 120$, and $z_s = 72$ with $\varphi = 0, 0.4167\pi, \pi$, and 1.4167π, (b) $N = 4$, $z_r = 125$, and $z_s = 73$ with $\varphi = 0, 0.505\pi, \pi$, and 1.505π. *Model from Inalpolat and Kahraman [33].

of the PGT system are observed. Subsequently, the effects of TPM applied in internal meshes on the dynamic tooth loads of the PGT system are investigated. At last, introducing the GA to obtain optimal TPM minimizing dynamic load fluctuation of the PGT system is discussed. It needs to be pointed out that the external torque applied to the planetary system keeps consistent in each operating condition.

According to the parameters of the three equally spaced planets' PGT system listed in Table 1, vibration properties can be obtained. The natural frequency and vibration mode of the PGT system is listed in Table 2. All vibration modes can be classified into torsional (R) and translational (T) modes, and the translational mode has two equal natural frequencies. This phenomenon agrees with the conclusion proposed by Lin et al. [30].

4.1. Effects of Modification Parameters. In this section, according to the NLSTE defined in equations (4)–(8) and the potential energy method suggested by Yang and Lin [11], quasi-static TVMS and LSTE are obtained with different TPM parameters. Considering the calculated TVMS and NLSTE as excitations of the planetary system defined by equations (16a), (16b), and (17a)–(17d), dynamic responses of the system can be solved by the Newmark-β method.

It is assumed that TPM parameters are only applied to sun-planet gear meshes, and the tooth profile of ring-planet gear meshes remains unmodified. Since working faces for sun-planet and ring-planet mesh on a planet gear is different, this assumption can therefore be guaranteed. Besides, tooth profile modification is only applied in the tip of the sun gear and planet gear, and all the geometric parameters and profile modification parameters are identical for all the planets. In the overall analyses, the input speed increases from 0 rpm to 9000 rpm and the input torque is 900 Nm.

4.1.1. Effects of Amount of TPM. In order to investigate the effects of the amount of TPM on dynamic response of the planetary gear trains, four cases with TPM are studied. Firstly, TVMS, LSTE, and NLSTE of a sun-planet gear mesh under different amount of modifications are shown in Figure 7. Four cases with different amounts of TPM $C_{a,1}$ taking 5 μm, 10 μm, 15 μm, and 20 μm are discussed. These four cases have the same normalized modification angle with $A_n = 1$, which implies the tip relief starts from HPSTC. Furthermore, these four cases are compared against the condition that no modification is applied to the gear meshes. The black line in Figure 7 refers gear tooth without modification, where the NLSTE equals zero during the overall mesh cycle and sudden jump occurs in the region between double- and single-tooth engagement of TVMS, as shown in Figure 7(b). NLSTE excitation appears when TPM is applied as illustrated in Figure 7(a). We define the region of the NLSTE greater than zero as the effective region for the NLSTE in a one mesh cycle. It can be found that the amplitude of the NLSTE is proportional to the value of the amount of TPM, but the effective region remains unchanged over the mesh cycle. Meanwhile, time-varying mesh stiffness gets smooth after TPM, as shown in Figure 7(b). However, the contact ratio and the mesh stiffness of the double-tooth engagement region decrease as C_a increases. It can be observed from Figure 7(c) that the value of the LSTE increases with the increase of C_a in the double-tooth engagement region, so that the peak-peak value of the LSTE can reach a minimum value with proper selection of amount of TPM. We obtain the minimum peak-peak value of the LSTE as 1.2 μm when $C_a = 10$ μm.

The dynamic deviation factors of external and internal meshes in the planetary system are exhibited in Figure 8. It can be observed that dynamic tooth loads get improved in most speed ranges for external meshes after TPM, as shown in Figure 8(a). Among these four TPM cases as displayed in

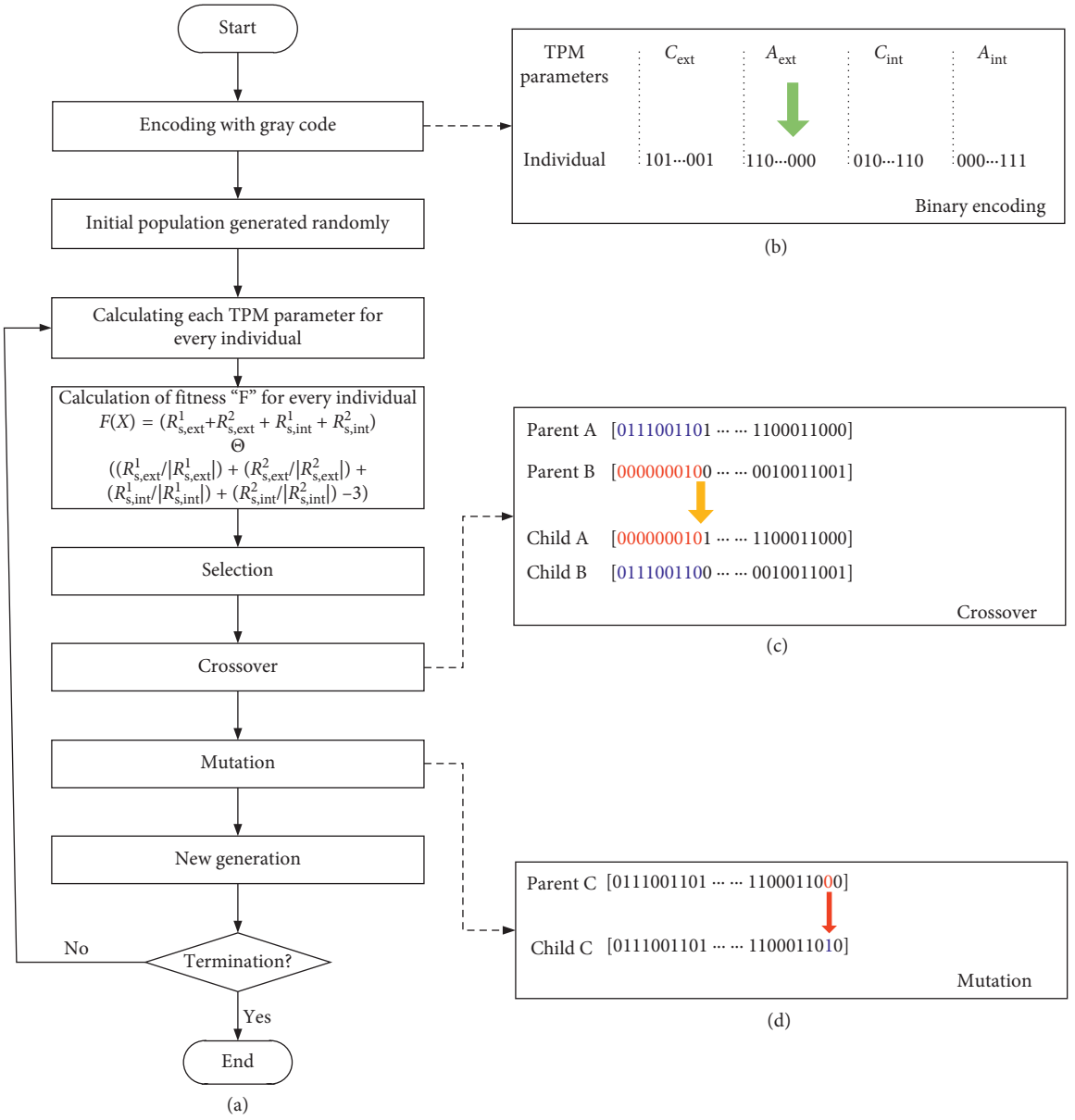

Figure 6: (a) Flowchart of the GA computational model; (b) encoding of individual; (c) crossover; (d) mutation.

Table 1: Basic parameters of the example PGT.

Parameter	Symbol and value
Number of teeth	$z_s = 32,\ z_p = 22,\ z_r = 76$
Module (mm)	$m = 4$
Pressure angle (°)	$\alpha_s = \alpha_r = 25$
Face width (mm)	$L_s = L_p = L_r = 40$
Young's modulus (GPa)	$E = 210$
Poisson's ratio	$\nu = 0.3$
Translational bearing stiffness (kN/mm)	$k_{sx} = k_{sy} = 100,\ k_{rx} = k_{ry} = 100,\ k_{cx} = k_{cy} = 100,\ k_{pn} = 100$
Rotational reaction stiffness (kNm/mrad)	$k_{ru} = 1000,\ k_{su} = k_{cu} = 0$

Figure 8(a), dynamic tooth loads get reduced over the entire speed range when $C_a = 5\,\mu$m and $10\,\mu$m. Particularly, we get the minimum value of the dynamic deviation factor over the entire speed range when $C_a = 10\,\mu$m. Dynamic tooth loads get reduced in most speed ranges except in the vicinity of sun-gear speed at 6300 rpm when $C_a = 15\,\mu$m. However,

Table 2: Natural frequencies (Hz) and vibration modes of the example PGT.

	f_1	f_2	f_3	f_4	f_5	f_6	f_7	f_8	f_9	f_{10}	f_{11}	f_{12}
Frequency	0	487 (2)	663 (2)	931(2)	1200	1334(2)	4551(2)	5550	5780	6108(2)	6802	13373
Mode	R	T	T	T	R	T	T	R	R	T	R	R

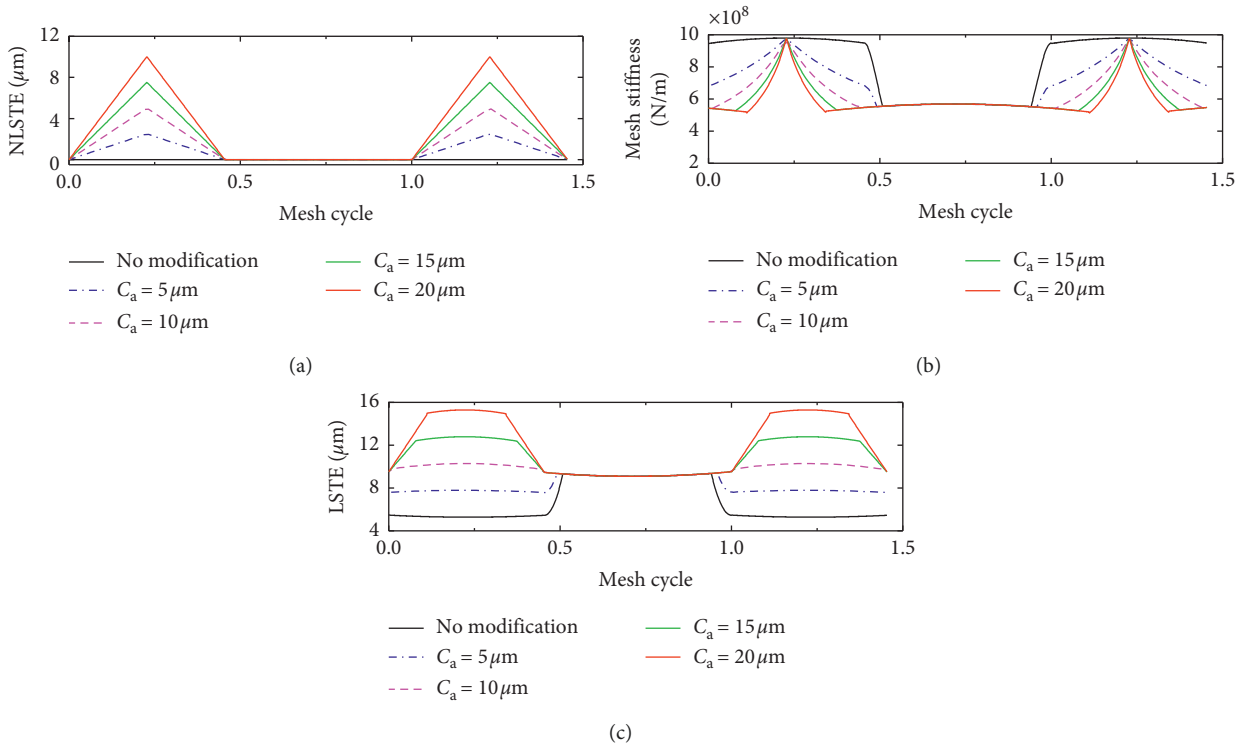

Figure 7: TVMS and TEs of a sun-planet mesh gear pair influence of the amount of TPM: (a) NLSTE, (b) TVMS, and (c) LSTE.

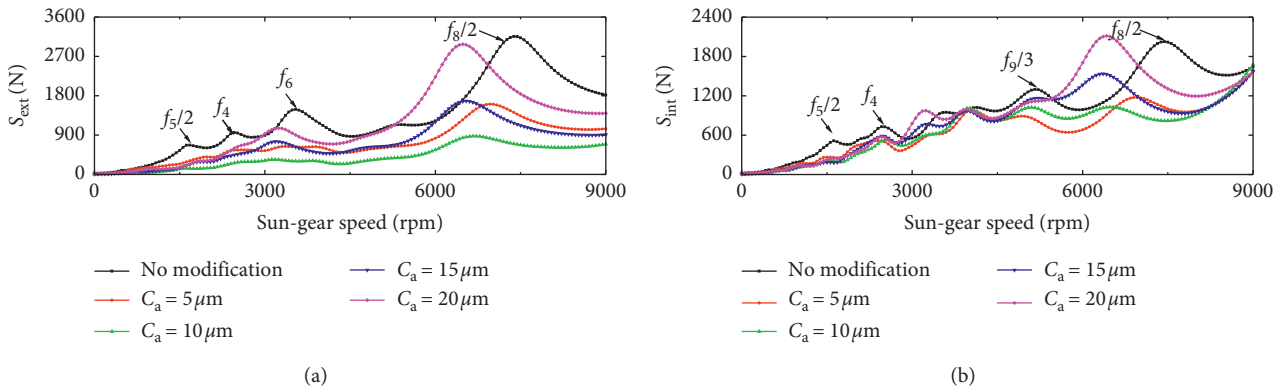

Figure 8: Dynamic tooth loads on external and internal meshes versus sun-gear speed influence of the amount of TPM: (a) sun-planet meshes and (b) ring-planet meshes.

dynamic tooth loads are not improved evidently and even become worse as sun-gear speed keeps increasing when $C_a = 20\,\mu m$. In addition, some response peaks can be found for different input speed. By comparing the mesh frequencies at different response peaks and the vibration properties of the PGT system in Table 2, the vibration mode which is excited can be obtained, as shown in Figure 8. The result shows that both the torsional and rotational vibration mode can be excited, and TPM can help reduce the vibration response amplitude effectively.

It is clear that proper TPM applied in external meshes can improve the dynamic behavior of external meshes.

Furthermore, an appropriate TPM scheme depends on minimum fluctuation of the LSTE. However, TPM applied in external meshes is unable to improve the dynamic tooth loads for internal meshes, as shown in Figure 8(b). Dynamic tooth loads for internal meshes get improved to a certain degree when $C_a = 5\,\mu$m and $10\,\mu$m, but the effect is not apparent. Dynamic responses of internal meshes get even worse in other two cases. Optimal selection of modification parameters requires improving dynamic behavior in both external and internal meshes.

Two summits are distinct in Figure 8 with the corresponding sun-gear speed at 6500 rpm and 7380 rpm. Effects of the amount of TPM on planetary responses at these two operating speeds are displayed in Figures 9 and 10. Variation range of mesh force and dynamic transmission error (DTE), defined in reference [3] by Tamminana and Kahraman, decrease first then increase with the increasing amount of TPM in external meshes as shown in Figures 9(a), 9(b), 10(a), and 10(b) and reach the minimum and maximum when $C_a = 10\,\mu$m and $15\,\mu$m, respectively. Sun-gear movement trajectory has similar law as the variation of amount of TPM, as shown in Figures 9(c) and 10(c). From Figures 9(a)–9(c), we can see that the variation range and maximum value of mesh force and DTE increases when $C_a = 20\,\mu$m. The sun-gear trajectory has the same phenomenon, which corresponds to the results displayed in Figure 8(a). Figure 10(a) shows that the narrower fluctuation range of external mesh force appears when $C_a = 20\,\mu$m, so that the dynamic tooth loads on external meshes get improved. However, the variation range, maximum value, and amplitude of sun-gear trajectory are higher; therefore, noise and vibration of the planetary system become more intensive when $C_a = 20\,\mu$m. The main reason is that excessive amount of TPM causes excessive initial tooth separation and results in a high-amplitude NLSTE so that sun gear requires moving more displacement in order to compensate the initial tooth errors. It indicates that even though improper modification parameters can improve dynamic tooth loads, unexpected situation would happen. If the best modification is not obtained, smaller amount of TPM are more acceptable than excessive amount of TPM.

4.1.2. Effects of Normalized Modification Angle. The effects of normalized modification angle A_n on time-varying mesh stiffness and transmission errors in external meshes are shown in Figure 11. Four cases of different A_n, taking 0.3, 0.5, 1, and 1.2, are studied. The amount of TPM takes $8\,\mu$m for different cases since $C_a = 8\,\mu$m can obtain the minimum fluctuation of LSTE when $A_n = 1$ in Section 4.1.1. When normalized modification angle is less than 0.5, the NLSTE equals zero and the peak-peak value of the LSTE remains almost unchanged, as illustrated in Figures 11(a) and 11(c). However, TVMS is affected seriously, where the mesh stiffness decreases in the double-tooth engagement region as the normalized modification angle increases and the contact ratio also gets reduced, as shown in Figure 11(b). When the normalized modification angle is greater than 0.5, the effects appear significantly different. Meanwhile, the amplitude and the effective region of the NLSTE arise. Furthermore, the peak-peak value of the LSTE decreases with the increase of the normalized modification angle, while TVMS varies very little, as displayed in Figures 11(a) and 11(c).

Figure 12 shows the effects of normalized modification angle on dynamic tooth loads. Similar with the results proposed in Section 4.1.1, TPM applied in external meshes can improve the dynamic tooth loads in external meshes. However, the dynamic tooth loads may become worse in internal meshes, as illustrated in Figure 12. At the entire sun-gear speed range, the dynamic tooth load in external meshes can be reduced apparently after TPM. It can be found that the dynamic deviation factor are quite approximate over the entire sun-gear speed range in external meshes when $A_n = 1$ and 1.2, except sun-gear speed locates between 5000 rpm and 9000 rpm, where $A_n = 1.2$ obtains better dynamic response, as displayed in Figure 13(a). It implies that $A_n = 1.2$ is the best modification scheme at the proposed sun-gear speed range for external meshes when $C_a = 8\,\mu$m.

Figure 13 shows the effect of the normalized modification angle on the dynamic response of the planetary system at sun-gear speed 6800 rpm, where the peak value of the dynamic deviation factor appears at external meshes for the above four cases with different A_n. The maximum value and variation of external mesh force are minimum for $A_n = 1.2$, as well as the variation of DTE of external meshes, as shown in Figures 13(a) and 13(b). Meanwhile, the amplitude of sun-gear radial trajectory gets the minimum when $A_n = 1.2$. It indicates that $A_n = 1.2$ is the best modification scheme for external meshes at sun-gear speed 6800 rpm, which coincides with the results illustrated in Figure 12(a). For internal meshes, TPM can reduce the dynamic vibration, as exhibited in Figure 13(d).

4.1.3. Effects of Modification Curve. Here, effects of the modification curve on TVMS and TEs are presented in Figure 14. Two different modification curve with identical amount of TPM $C_a = 8\,\mu$m and normalized modification angle $A_n = 1.2$ are analyzed. It is clear that parabolic modification has lower amplitude of the NLSTE and equal effective region compared with linear modification, as shown in Figure 14(a). Interestingly, it can be found that TVMS for linear and parabolic modification is almost identical, as illustrated in Figure 14(b). The peak-peak value of the LSTE for parabolic modification is smaller than linear modification, as displayed in Figure 14(c).

Then, the effects of the modification curve on dynamic response of the planetary system are shown in Figure 15. From Figure 15(a), it can be observed that both linear and parabolic modification can improve the dynamic tooth loads for external meshes over the entire sun-gear speed range. The dynamic tooth load for parabolic modification appears to be better than linear modification for external meshes. Dynamic tooth loads for internal meshes are also getting improved over the entire input speed range. But the improvement is as significant as external meshes. Dynamic response even increases slightly in some speed area. In addition, it is difficult to judge whether linear or parabolic

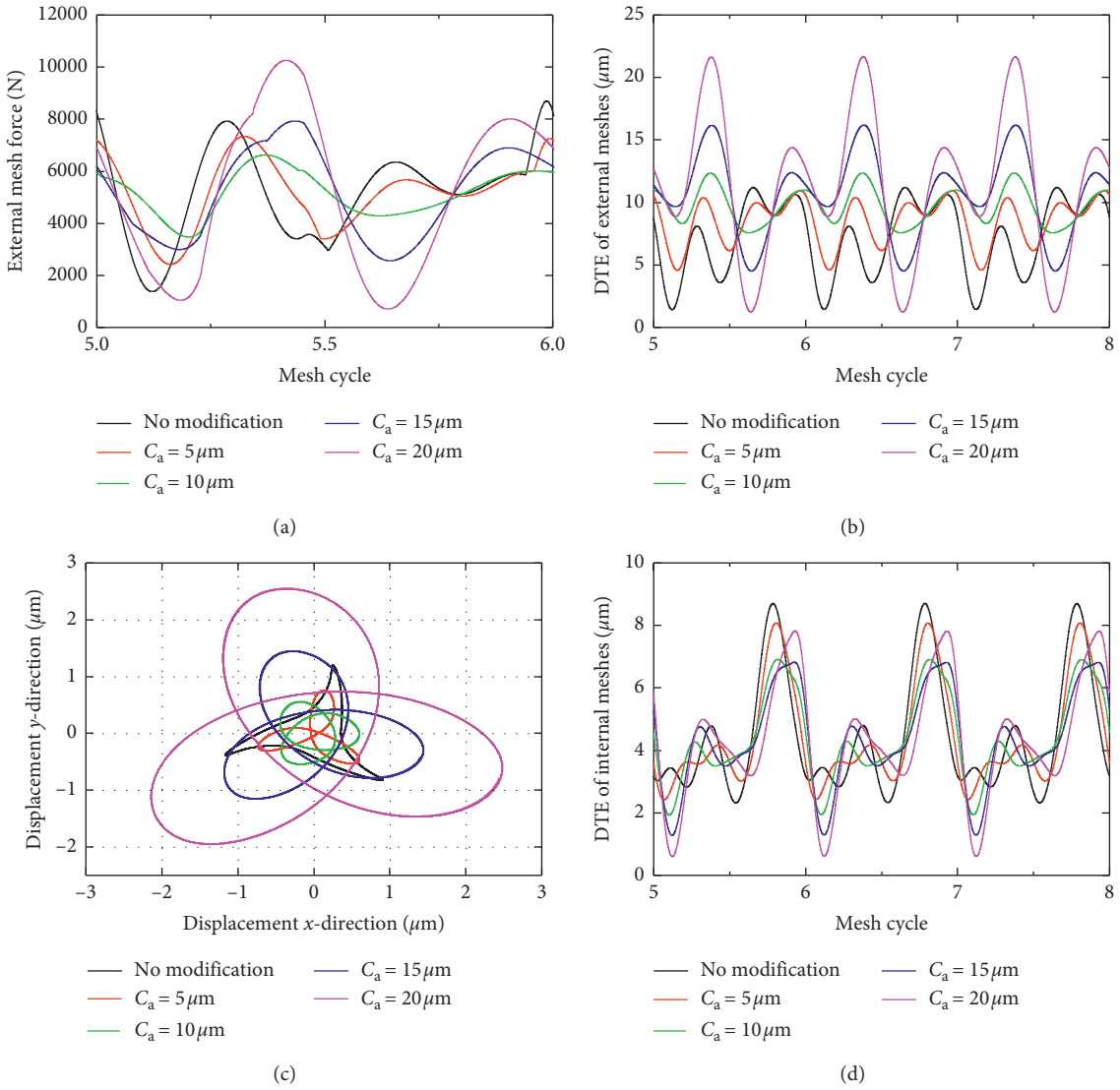

Figure 9: Dynamic responses for different amounts of TPM on external and internal meshes at sun-gear speed 6500 rpm: (a) dynamic mesh force; (b) DTE of sun-planet meshes; (c) sun-gear trajectory; (d) DTE of ring-planet meshes.

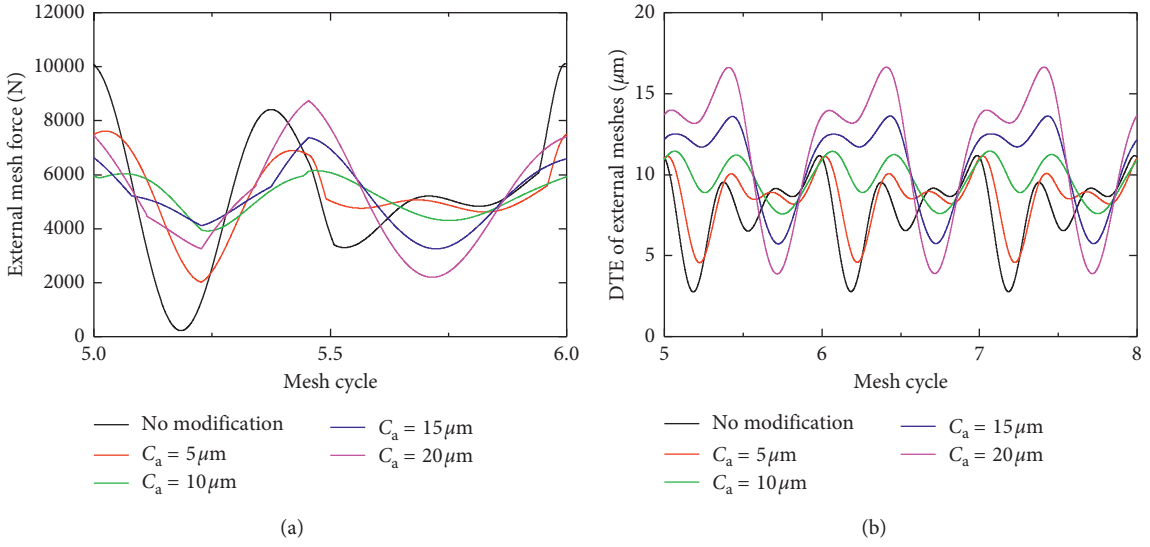

Figure 10: Continued.

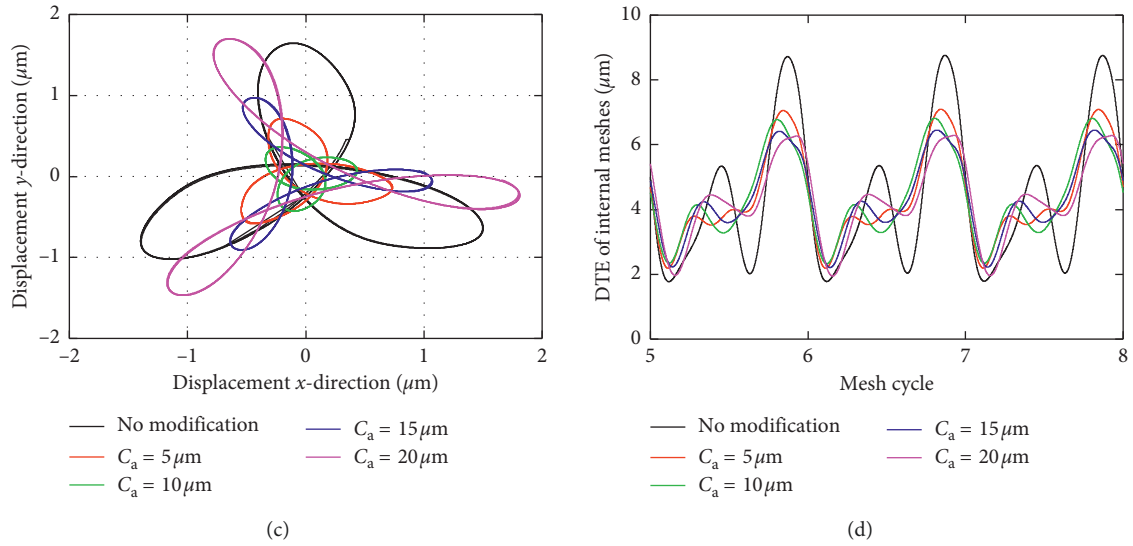

Figure 10: Dynamic responses for different amounts of TPM on external and internal meshes at sun-gear speed 7380 rpm: (a) dynamic mesh force; (b) DTE of sun-planet meshes; (c) sun-gear trajectory; (d) DTE of ring-planet meshes.

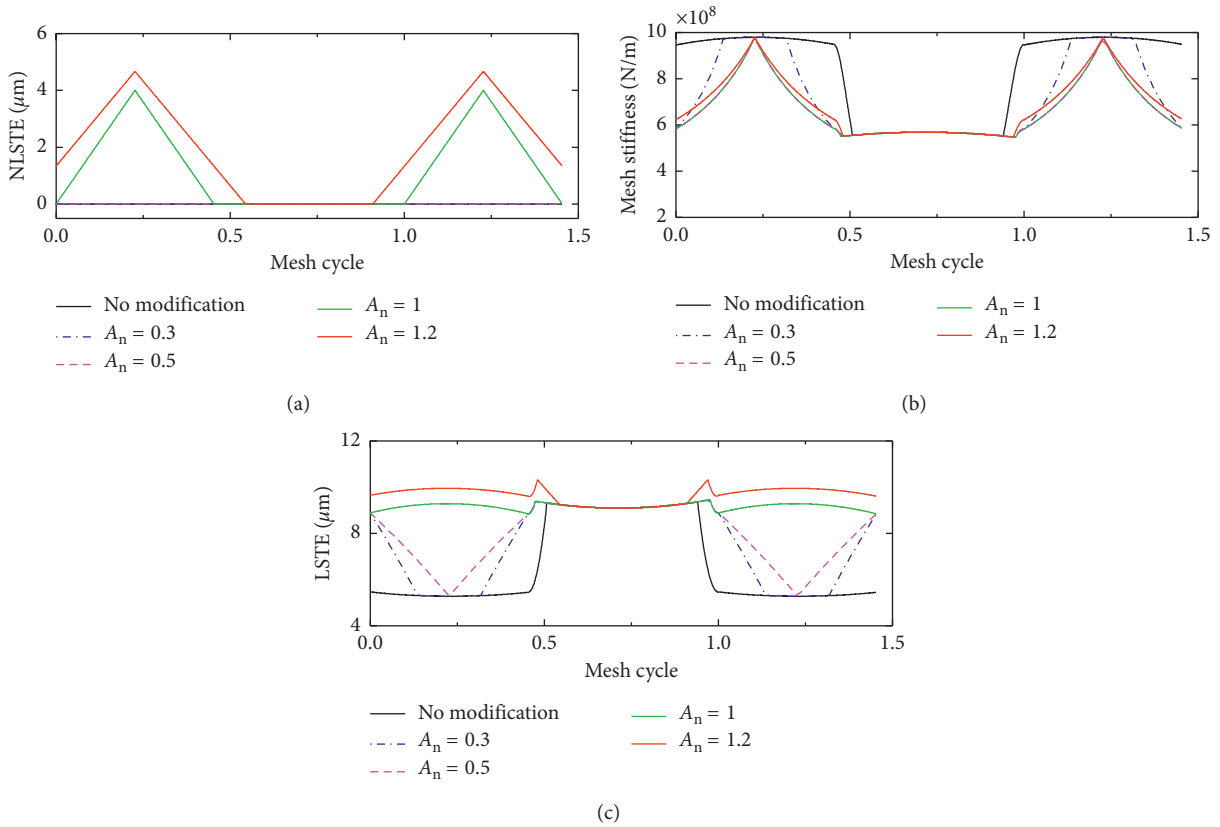

Figure 11: TVMS and TEs of a sun-planet mesh gear pair influence of the normalized modification angle: (a) NLSTE; (b) TVMS; (c) LSTE.

TPM applied at external meshes is better for internal meshes. Investigation of TPM effects on internal meshes need to be further conducted.

According to the results illustrated form Section 4.1.1 to Section 4.1.3, we can observe that TPM applied to external meshes can improve the dynamic load for external meshes, but the effect for internal meshes is always negative. Besides, TPM applied in external meshes with lower peak-peak value of the LSTE can improve the dynamic tooth loads better for external meshes. This indicates that the lower peak-peak

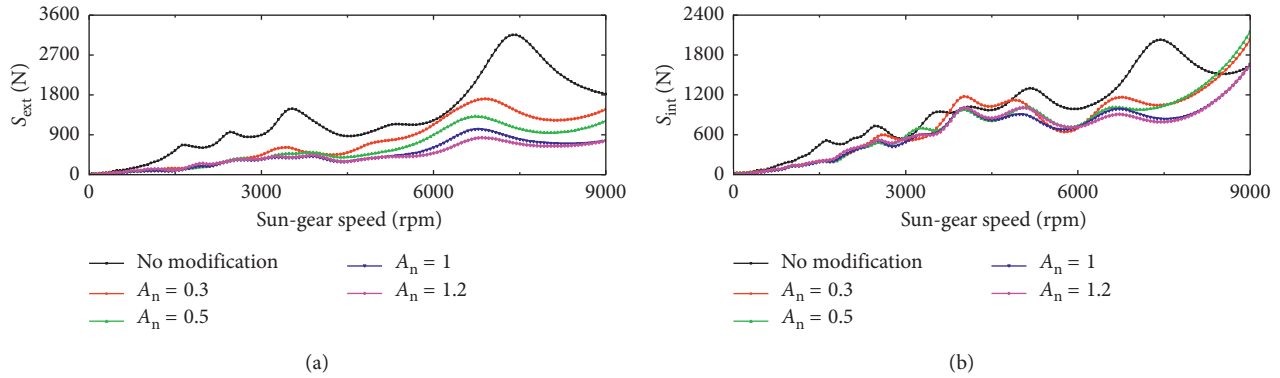

FIGURE 12: Dynamic tooth loads on external and internal meshes versus sun-gear speed influence of the normalized modification angle: (a) sun-planet meshes and (b) ring-planet meshes.

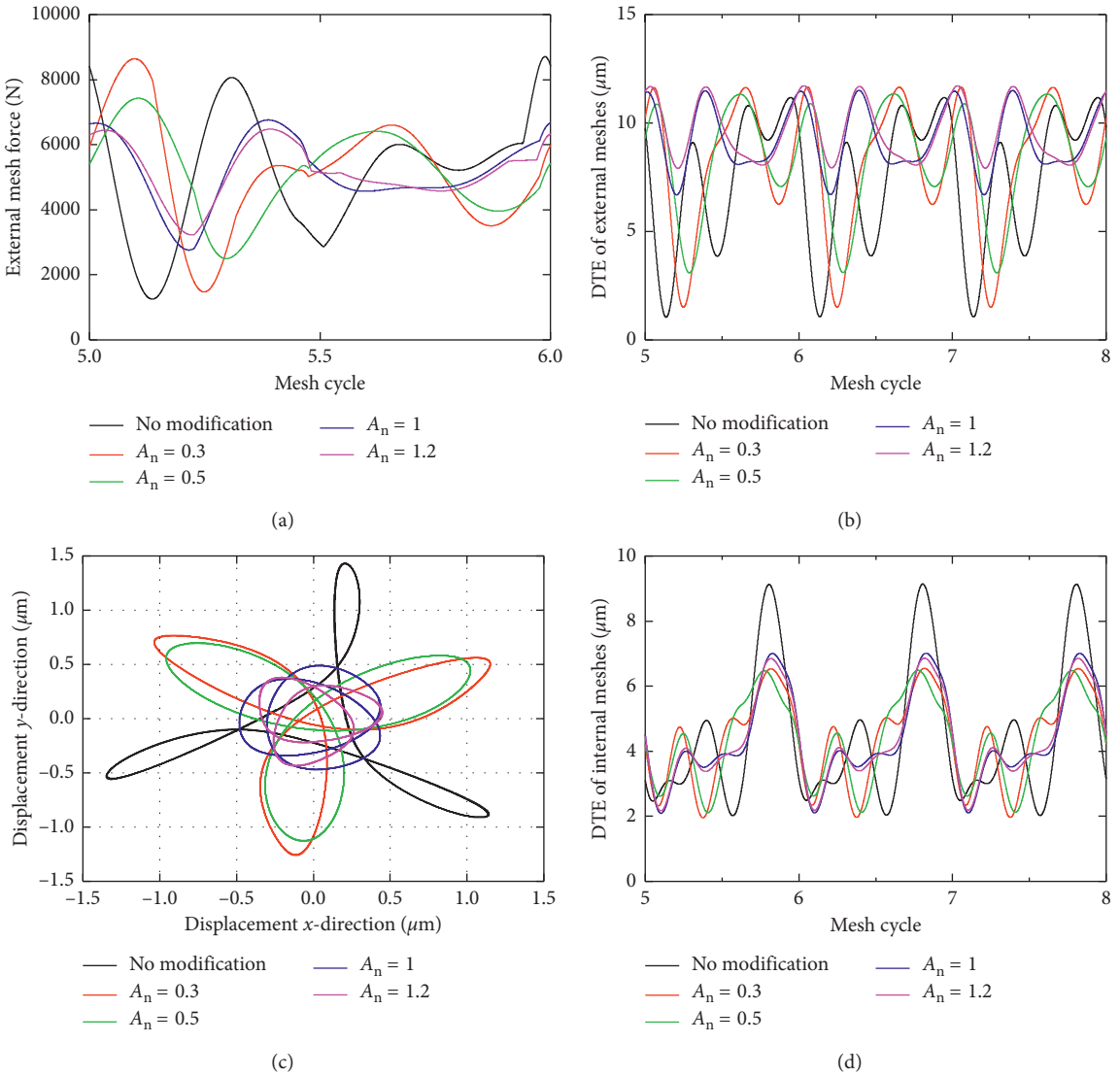

FIGURE 13: Dynamic responses for different normalized modification angles on external and internal meshes at sun-gear speed 6800 rpm: (a) dynamic mesh force; (b) DTE of sun-planet meshes; (c) sun-gear trajectory; (d) DTE of ring-planet meshes.

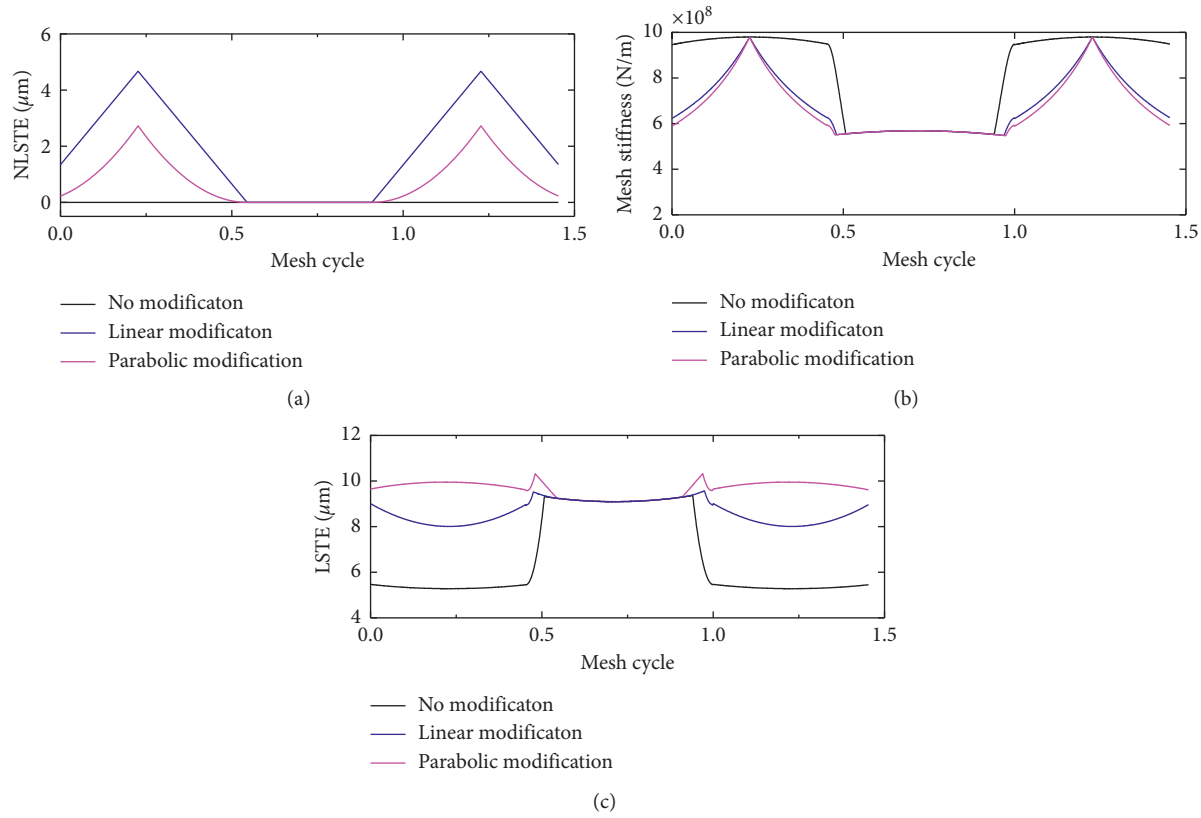

Figure 14: TVMS and TEs of a sun-planet mesh gear pair influence of the modification curve: (a) NLSTE; (b) TVMS; (c) LSTE.

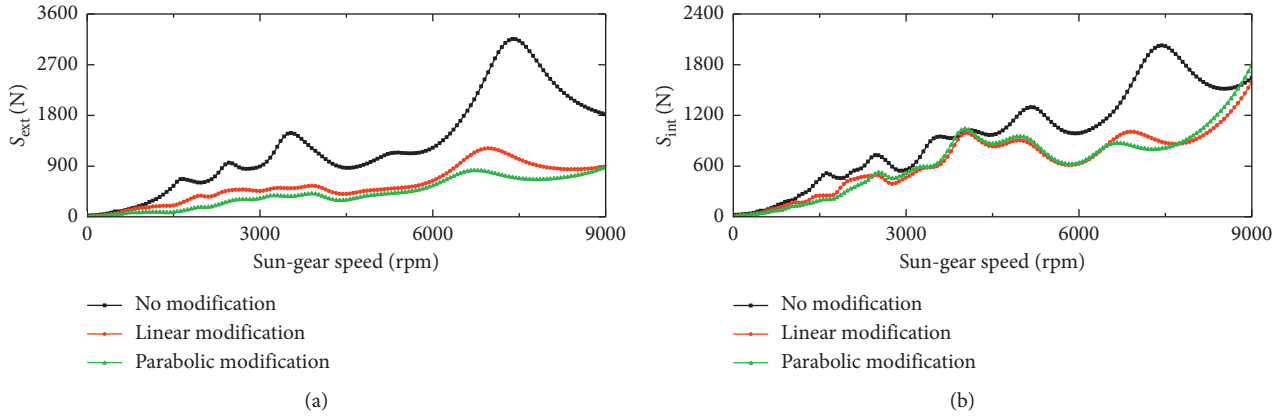

Figure 15: Dynamic tooth loads on external and internal meshes versus sun-gear speed influence of the modification curve: (a) sun-planet meshes and (b) ring-planet meshes.

value of the LSTE in internal meshes can analogously improve the dynamic tooth loads for internal meshes. In order to demonstrate the variation of the peak-peak value of the LSTE with TPM better, the relative peak-peak value of the LSTE is defined as follows [7]:

$$R_p = \frac{P_m - P_n}{P_n} \times 100\%, \quad (24)$$

where R_p denotes the relative peak-peak value of the LSTE and P_m and P_n represent the peak-peak value of the LSTE with and without TPM, respectively.

Figure 16 shows the relative peak-peak value of the LSTE, which varies with the amount of TPM and normalized modification angle for external and internal meshes under linear and parabolic modification. The coordinate corresponding to the modification parameters for the minimum relative peak-peak value of the LSTE is marked in Figure 16. It is evident that when the normalized modification angle is less than 0.5, the amount of TPM has tiny effect on the relative peak-peak value of the LSTE R_p for both external and internal meshes. But R_p reduces when normalized modification keeps arising. Moreover, when the normalized

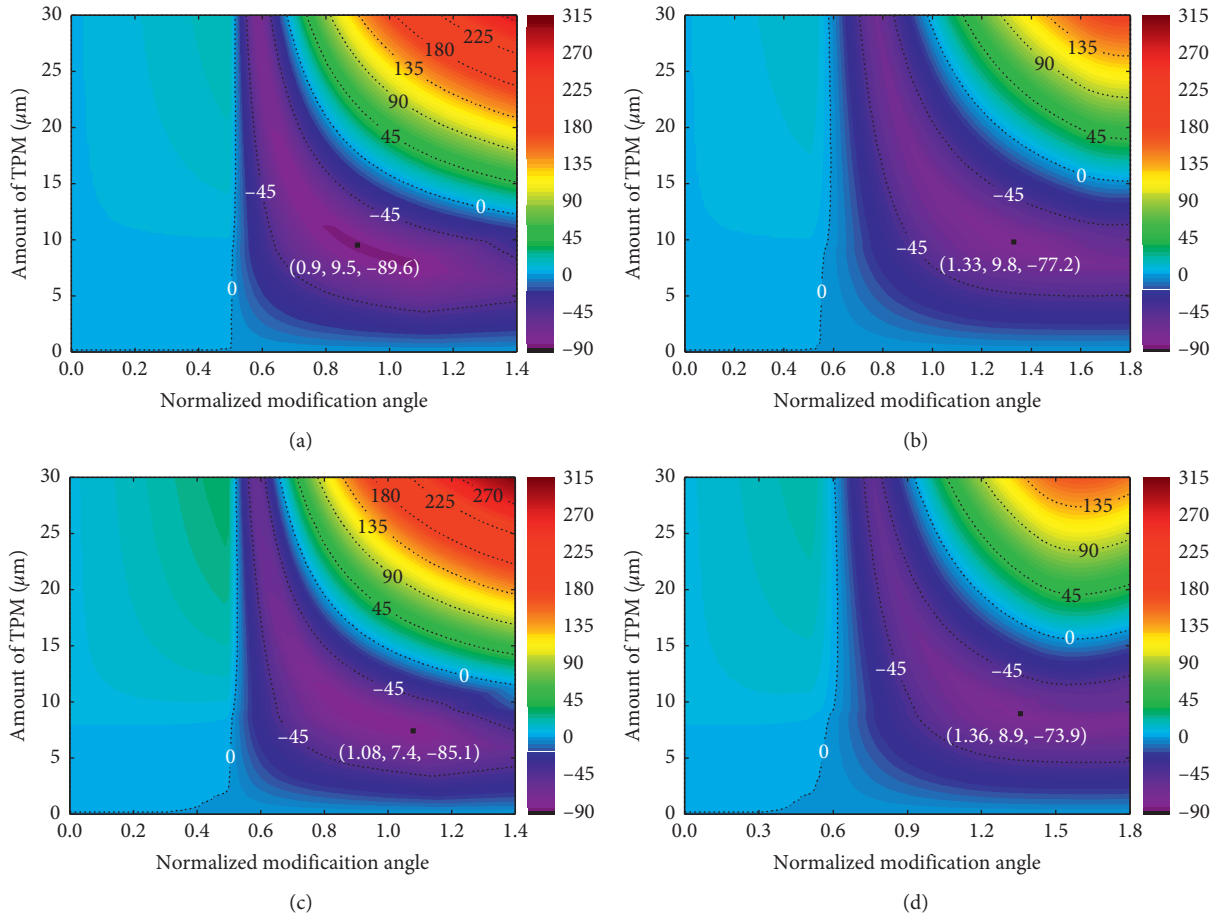

FIGURE 16: Relative peak-peak value of the LSTE (unit:%): (a) external meshes with linear modification, (b) external meshes with parabolic modification, (c) internal meshes with linear modification, and (d) internal meshes with parabolic modification.

modification angle is defined (greater than 0.5), R_p declines rapidly at first, then goes up fast with the increasing amount of TPM for both external and internal meshes in linear modification. However, R_p changes more slowly in parabolic modification as displayed in Figure 16. And this principle is also suitable for the influence of the normalized modification angle in linear and parabolic modification when the amount of TPM is defined. According to the minimum R_p marked in Figure 16, it can be found that minimum R_p is smaller in linear modification for external and internal meshes, and its corresponding amount of TPM and normalized modification angle are also smaller compared with parabolic modification.

4.2. Effects of Profile Modification Applied in Ring-Planet Gear Mesh. As illustrated in Section 4.1, proper TPM improves the dynamic load of external meshes over the entire sun-gear speed range. In order to investigate the influence of TPM applied to internal meshes on the dynamic response of the PGT, two sun-gear rotating speed 3000 rpm and 7500 rpm are selected, which correspond to the trough and crest of the dynamic deviation factor without TPM for external and internal meshes, respectively. It should be pointed out that external torques applied to the system equals 900 Nm and linear TPM only applied to internal meshes with identical amount of TPM and normalized modification angle in ring gear and all planet gears. Figure 17 illustrates the contour plot of the relative deviation factor in external and internal meshes defined in equations (20a) and (20b). Obviously, when sun-gear speed is at 3000 rpm, the region of TPM parameters improving dynamic tooth loads for internal meshes is quite limited as illustrated in Figure 17(b). Meanwhile, three minimum points can be obtained in the contour plot, which is marked as A, B, and C, respectively. Although many TPM parameters are unaccepted for internal meshes, dynamic tooth loads get improved for external meshes, as displayed in Figures 17(a) and 17(b). When sun-gear operates at 7500 rpm, acceptable modification parameters region gets wider for internal meshes. However, acceptable parameters region gets smaller for external meshes compared with the sun-gear speed at 3000 rpm, as exhibited in Figures 17(c) and 17(d).

For external meshes, reduction of the peak-peak value of the LSTE can improve the dynamic tooth loads for external meshes as mentioned in Section 4.1. In order to investigate the relationship among the peak-peak value of LSTE, TVMS, and the dynamic response of the planetary system, four modification parameters are studied as shown in Table 3.

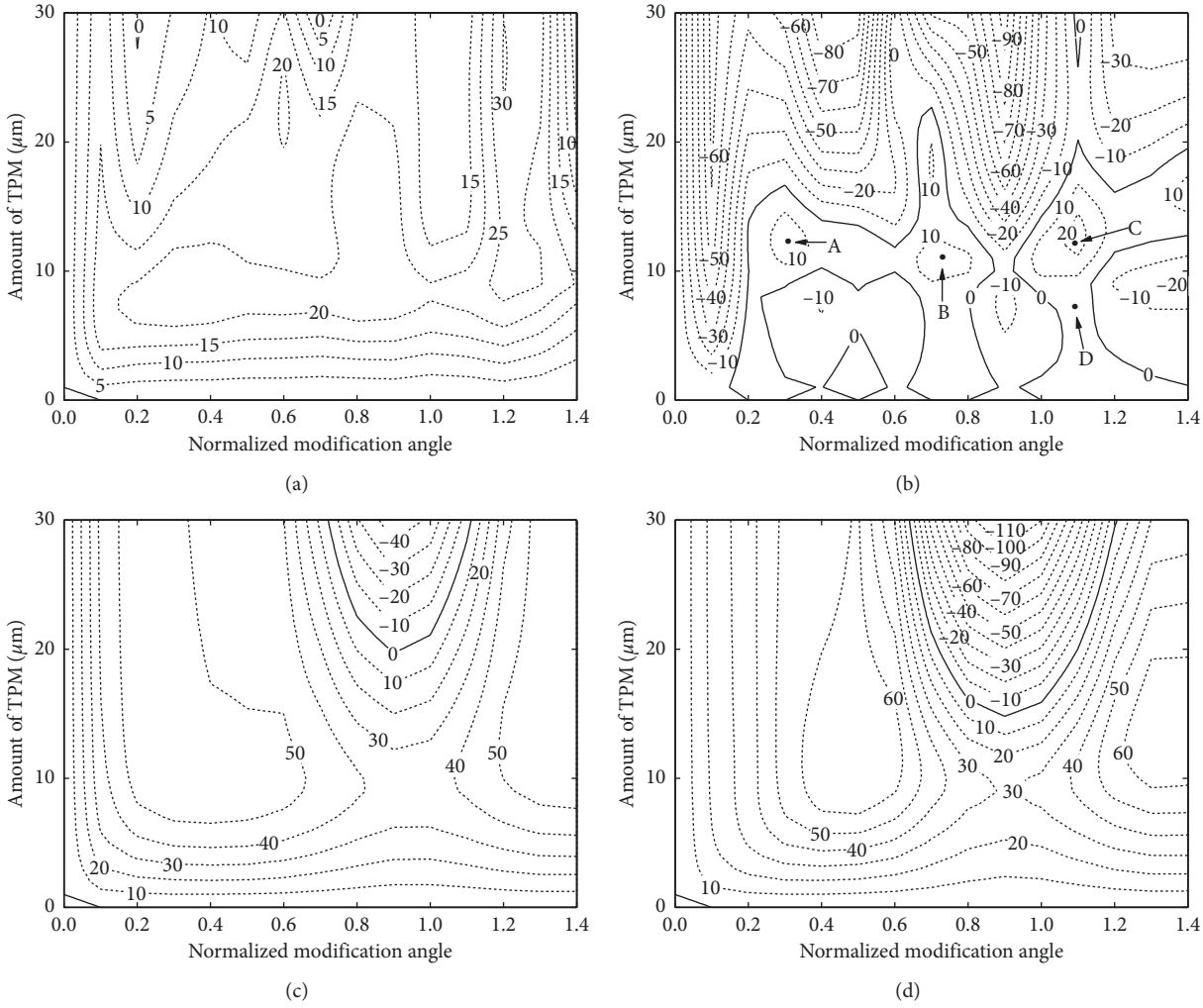

Figure 17: Dynamic tooth loads on external and internal meshes under different sun-gear speed effects of TPM applied in internal meshes (unit:%): (a) external meshes, (b) internal meshes at 3000 rpm, (c) external meshes, and (d) internal meshes at 7500 rpm.

Table 3: Modification parameters and relative peak-peak value of the LSTE of the noted point.

Point	A	B	C	D
Amount of TPM (μm)	12.4	10.8	12.3	7.2
Normalized modification angle	0.31	0.72	1.09	1.08
Relative peak-peak value of LSTE (%)	11.9	−65.6	−18.5	−85.1

Meanwhile, these four modification parameters are noted in Figure 17(b) as A, B, and C, while point D stands for the modification parameters with the minimum relative peak-peak value of the LSTE, as shown in Figure 16(c). NLSTE, TVMS, and LSTE in these four points are displayed in Figure 18. Variation laws of NLSTE, TVMS, and NLSTE with TPM parameters obey the principle mentioned in Section 4.1.

Figure 19 illustrates the dynamic tooth loads for external and internal meshes at different modification parameters, as shown in Table 3. From Figure 19(a), we can observe that point C is the only one that improves the dynamic tooth loads over the entire speed range for internal meshes, while the other three points will increase dynamic tooth loads in some sun-gear speed range. However, performance in these four points varies considerably at various sun-gear speed ranges. For instance, when sun-gear speed ranges from 2100 rpm to 3200 rpm and 4300 rpm and 6700 rpm, point C improves the dynamic tooth loads best. But when sun-gear speed ranges from 3500 rpm to 4100 rpm and 6800 rpm to 7800 rpm, point A behaves best, as shown in Figure 19(b). It implies that optimal modification schemes depend on the operating speed with regard to internal meshes. Point D refers to the minimum peak-peak value of the LSTE in external meshes, as illustrated in Figure 16(c). Meanwhile, point B reduces the peak-peak value of the LSTE quite a lot. However, points B and D are unable to improve their dynamic behavior very well for internal meshes, becoming even worse than point C. Therefore, unlike external meshes, optimal modification parameters are not determined only by the peak-peak value of the LSTE in internal meshes. From Figure 19(a), it can be observed that when TPM is applied in internal meshes, dynamic tooth loads for external meshes might become better or worse.

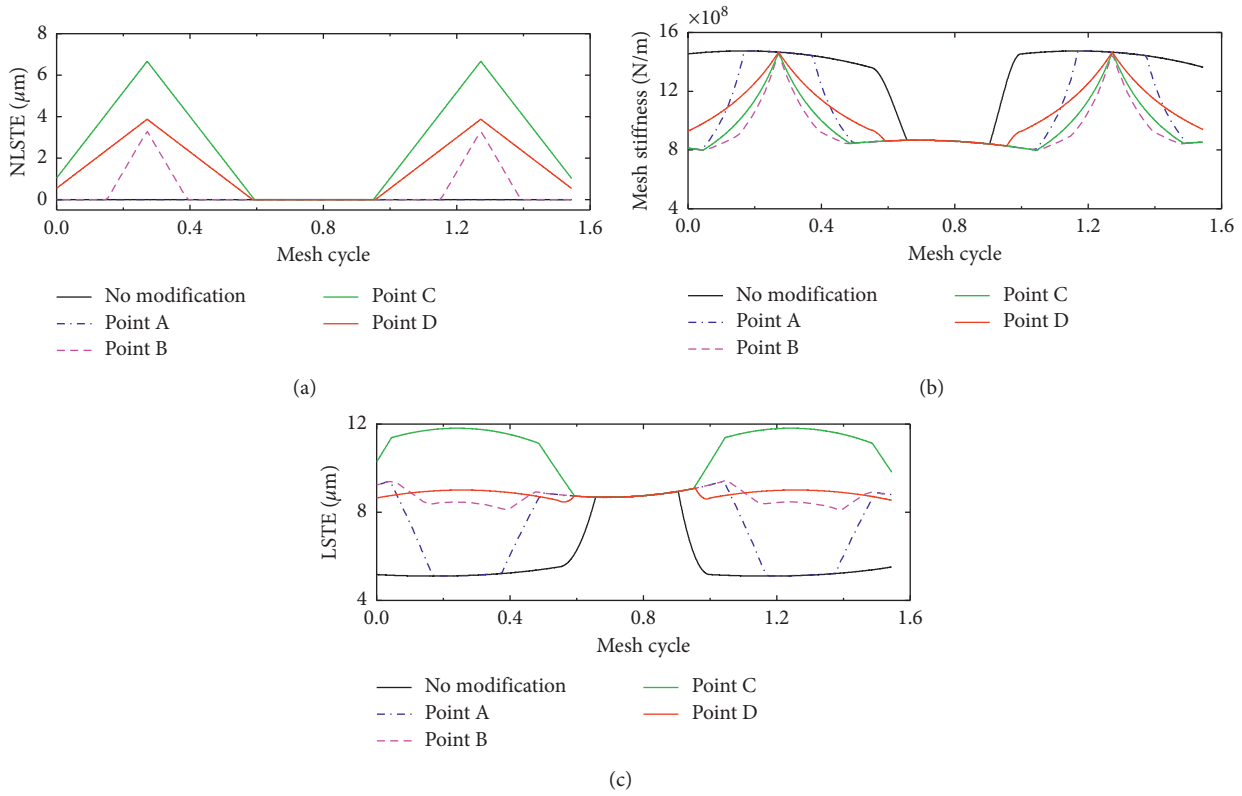

Figure 18: Time-varying mesh stiffness and transmission errors of a ring gear-mesh gear pair at different points: (a) no-load static transmission error, (b) time-varying mesh stiffness, and (c) loaded static transmission error.

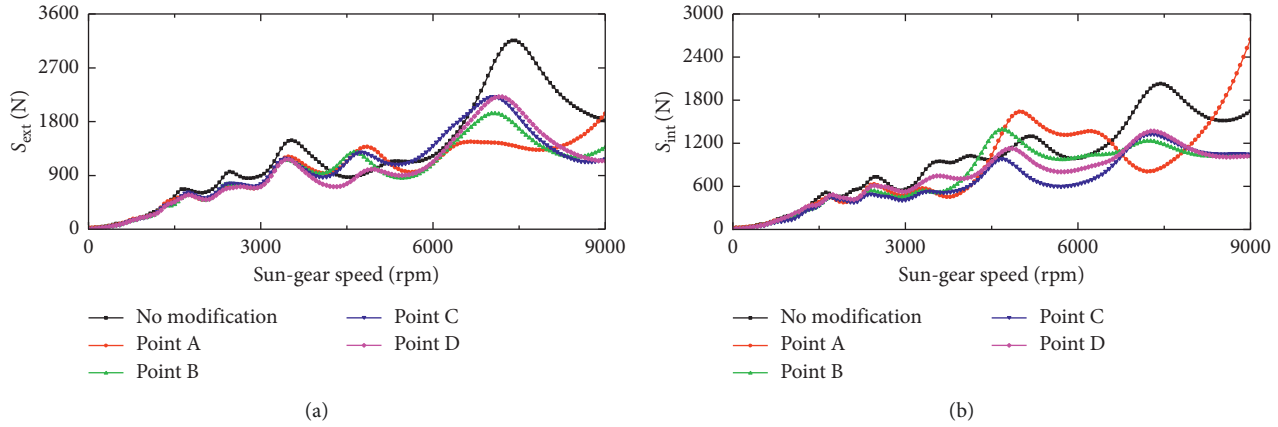

Figure 19: Dynamic tooth loads on external and internal meshes versus sun-gear speed TPM applied in internal meshes: (a) ring-planet meshes and (b) sun-planet meshes.

4.3. Optimization of TPM for Dynamic Responses Reduction. Based on the results presented above, it can be found that optimal TPM for external meshes can increase the dynamic tooth loads on internal meshes, and this phenomenon also suits for internal meshes. In order to reduce the dynamic tooth loads in both external and internal meshes, TPM should be applied to both external and internal meshes simultaneously. It is supposed that TPM parameters are identical for all sun-planet gear meshes, as well as all ring-planet gear meshes. Dynamic tooth loads of external and internal meshes vary with four TPM parameters, amount of TPM, and normalized modification angle for both external and internal meshes.

As mentioned previously, there are strong relationship between TPM parameters and dynamic response of the planetary system. Optimal TPM can be obtained by the enumeration method which aims at obtaining the minimum vibration and dynamic response of the PGT. However, it is extremely time consuming and blindness. In recent research studies, it is confirmed that the GA is an effective method to

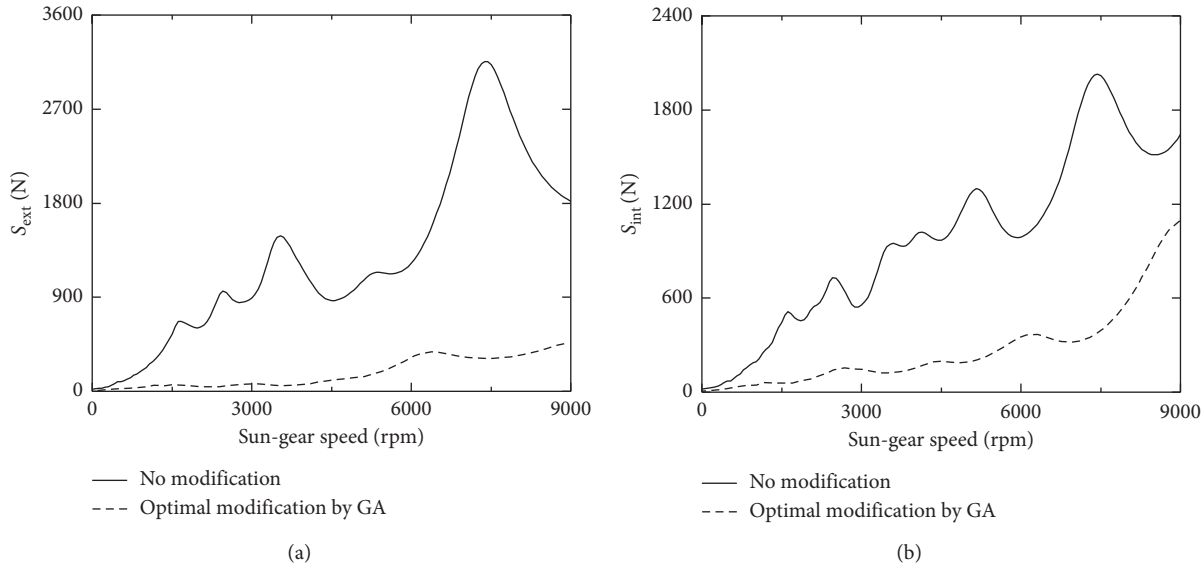

Figure 20: Dynamic tooth loads for (a) external meshes and (b) internal meshes of no modification (black line) and optimal modification by the GA (dash line).

find the optimal TPM [22, 35]. In order to achieve the optimal TPM, the GA is adopted in this study.

The presented GA is based on binary encoding with the four parameters mentioned above. It is assumed that the variation range of each parameter is the same for external and internal meshes. The amount of TPM ranges from 0 to 30 μm, and the normalized modification angle ranges from 0 to 1.4. Linear modification is employed. Step size of the amount of TPM and normalized modification angle chooses $\Delta C_a = 0.1\,\mu$m and $\Delta A_n = 0.01$, respectively. Therefore, each individual in the GA consists of four chromosomes and each chromosome represents one modification parameter. Chromosomes of the amount of TPM and normalized modification angle have 9 genes ($2^8 < 301 < 2^9$) and 8 genes ($2^7 < 152 < 2^8$), respectively.

With regard to optimal TPM, it implies that the external and internal tooth loads decrease over the wide range of the sun-gear speed. However, it is unrealistic if the vibration response in the entire sun-gear speed range of every individual requires to be calculated. In order to evaluate the effectiveness of TPM, reduction of dynamic tooth loads in external and internal meshes at two sun-gear rotation speed are selected, which corresponds to the first two peak amplitude of dynamic tooth loads without TPM. As a result, 3540 rpm and 7400 rpm sun-gear speed are selected for external meshes and 5160 rpm and 7400 rpm for internal meshes. The presented GA improves the solutions by means of a certain number of iterations on a population with 20 individuals. Probability of crossover and mutation takes, respectively, 0.6 and 0.033 [22]. Based on these parameters of the GA, optimal simulation program can be performed in MATLAB. The simulation found that the value of fitness function converges after 300 iterations.

Figure 20 shows the dynamic deviation factors of external and internal meshes with TPM parameters which stem from the GA. Black line represents results without TPM, and dash line represents the optimal modification scheme from the GA. It can be found that dynamic tooth load has been greatly reduced for external and internal meshes and no obvious peak appears over the entire sun-gear speed range. Furthermore, the optimal modification scheme behaves much better than the modification scheme illustrated in Sections 4.1 and 4.2. It implies that TPM applied only to external or internal meshes can hardly obtain a suitable modification scheme and both external and internal meshes should be taken into account in obtaining optimal TPM.

5. Conclusions

This paper focuses on the analysis of the effects of TPM on the dynamic response of the PGT. Considering the influence of gear tooth errors and TPM, an analytical mesh stiffness model is developed, and TVMS, LSTE, and NLSTE of an external mesh under different TPM parameters are analyzed. Based on the TVMS and gear mesh displacement along the line of action, a linear time-varying planetary gear dynamic model is proposed. For convenient evaluating dynamic response of the PGT, the dynamic deviation factor is introduced. The dynamic deviation factor under different TPM conditions is given. Effects of TPM on the dynamic response of PGT are analyzed in detail. In order to obtain the optimal TPM minimizing the dynamic response of the planetary, the GA is adopted. The main conclusions can be summarized as follows:

(1) TPM can make tooth engagement process smooth at double- and single-tooth alternating mesh. The gear contact ratio also increases in a certain degree after TPM. TVMS, LSTE, and NLSTE alter a lot after TPM, especially in double-tooth engagement region. The minimum peak-peak value of the LSTE can be obtained with proper selection of TPM parameters.

TVMS for linear and parabolic TPM almost has no difference when the amount of TPM and normalized modification angle are defined. When the normalized modification angle is less than 0.5, the relative peak-peak value of the LSTE almost remains unchanged for arbitrary amount of TPM. When normalized modification angle is greater than 0.5, the relative peak-peak value of the LSTE would be influenced by the amount of TPM and normalized modification angle and varies more rapidly in linear TPM than parabolic TPM. Furthermore, the minimum peak-peak value of the LSTE is smaller in linear TPM and the corresponding amount of TPM and normalized modification also turns out to be smaller.

(2) TPM applied to external meshes can improve dynamic tooth loads in external meshes, while dynamic tooth loads in internal meshes might get worse. If only external meshes are taken into consideration, the smaller peak-peak value of the LSTE can improve the dynamic tooth loads better for external meshes. For some TPM parameters, even though dynamic tooth loads in external meshes get improved, bearing force will increase unfavorably. Proper TPM for internal meshes can increase the dynamic load in external meshes, which is similar to the phenomenon TPM applied in external meshes. However, dynamic response for internal meshes seems to be quite complicated, even the minimum peak-peak value of the LSTE is unable to reduce the dynamic response in internal meshes in some sun-gear speed range.

(3) It is proved that the GA is an effective method to obtain the optimal TPM for the minimum dynamic tooth loads for PGT. Optimal TPM can significantly reduce the dynamic tooth loads for external and internal meshes over the entire speed range, which can hardly be realized by TPM which is only applied in external or internal meshes.

Data Availability

The data used to support the findings of this study have not been made available because they are confidential.

Conflicts of Interest

The authors declare that they have no conflicts of interest.

Acknowledgments

This work was financially supported by the Key Project of Shandong Provincial Natural Science Foundation, China (no. ZR2019MEE029), Shandong Provincial Agricultural Machinery Equipment Research and Development Innovation Project (no. 2018YF018), the National Natural Science Foundation of China (Grant number: 51705012). The authors also acknowledge the support of the Beijing Key Laboratory for High-efficient Power Transmission and System Control of New Energy Resource Vehicle and the Fundamental Research Funds for the Central Universities.

References

[1] S. Li, "Gear contact model and loaded tooth contact analysis of a three-dimensional, thin-rimmed gear," *Journal of Mechanical Design*, vol. 124, no. 3, pp. 511–517, 2002.

[2] J. Wang and I. Howard, "Finite element analysis of high contact ratio spur gears in mesh," *Journal of Tribology*, vol. 127, no. 3, pp. 469–483, 2005.

[3] V. K. Tamminana, A. Kahraman, and S. Vijayakar, "A study of the relationship between the dynamic factors and the dynamic transmission error of spur gear pairs," *Journal of Mechanical Design*, vol. 129, no. 1, pp. 75–84, 2007.

[4] A. F. Del Rincon, F. Viadero, M. Iglesias, P. García, A. De-Juan, and R. Sancibrian, "A model for the study of meshing stiffness in spur gear transmissions," *Mechanism and Machine Theory*, vol. 61, pp. 30–58, 2013.

[5] A. Fernández, M. Iglesias, A. de-Juan, P. García, R. Sancibrián, and F. Viadero, "Gear transmission dynamic: effects of tooth profile deviations and support flexibility," *Applied Acoustics*, vol. 77, pp. 138–149, 2014.

[6] P. Velex and M. Maatar, "A mathematical model for analyzing the influence of shape deviations and mounting errors on gear dynamic behaviour," *Journal of Sound and Vibration*, vol. 191, no. 5, pp. 629–660, 1996.

[7] Z. Chen and Y. Shao, "Mesh stiffness calculation of a spur gear pair with tooth profile modification and tooth root crack," *Mechanism and Machine Theory*, vol. 62, pp. 63–74, 2013.

[8] H. Ma, X. Pang, R. Feng, J. Zeng, and B. Wen, "Improved time-varying mesh stiffness model of cracked spur gears," *Engineering Failure Analysis*, vol. 55, pp. 271–287, 2015.

[9] X. Xu, J. Lai, C. Lohmann, P. Tenberge, M. Weibring, and P. Dong, "A model to predict initiation and propagation of micro-pitting on tooth flanks of spur gears," *International Journal of Fatigue*, vol. 122, pp. 106–115, 2019.

[10] R. W. Cornell, "Compliance and stress sensitivity of spur gear teeth," *Journal of Mechanical Design*, vol. 103, no. 2, pp. 447–459, 1981.

[11] D. C. H. Yang and J. Y. Lin, "Hertzian damping, tooth friction and bending elasticity in gear impact dynamics," *Journal of Mechanisms, Transmissions, and Automation in Design*, vol. 109, no. 2, pp. 189–196, 1987.

[12] S. Wu, M. J. Zuo, and A. Parey, "Simulation of spur gear dynamics and estimation of fault growth," *Journal of Sound and Vibration*, vol. 317, no. 3–5, pp. 608–624, 2008.

[13] P. Sainsot, P. Velex, and O. Duverger, "Contribution of gear body to tooth deflections—a new bidimensional analytical formula," *Journal of Mechanical Design*, vol. 126, no. 4, pp. 748–752, 2004.

[14] F. Chaari, T. Fakhfakh, and M. Haddar, "Analytical modelling of spur gear tooth crack and influence on gearmesh stiffness," *European Journal of Mechanics-A/Solids*, vol. 28, no. 3, pp. 461–468, 2009.

[15] Z. Chen and Y. Shao, "Dynamic simulation of planetary gear with tooth root crack in ring gear," *Engineering Failure Analysis*, vol. 31, pp. 8–18, 2013.

[16] H. Ma, R. Song, X. Pang, and B. Wen, "Time-varying mesh stiffness calculation of cracked spur gears," *Engineering Failure Analysis*, vol. 44, pp. 179–194, 2014.

[17] S. Xue and I. Howard, "Dynamic modelling of flexibly supported gears using iterative convergence of tooth mesh stiffness," *Mechanical Systems and Signal Processing*, vol. 80, pp. 460–481, 2016.

[18] S. Xue, R. Entwistle, I. Mazhar, and I. Howard, "The spur planetary gear torsional stiffness and its crack sensitivity

under quasi-static conditions," *Engineering Failure Analysis*, vol. 63, pp. 106–120, 2016.

[19] R. G. Parker and J. Lin, "Mesh phasing relationships in planetary and epicyclic gears," *Journal of Mechanical Design*, vol. 126, no. 2, pp. 365–370, 2004.

[20] X. Liang, M. J. Zuo, and M. Pandey, "Analytically evaluating the influence of crack on the mesh stiffness of a planetary gear set," *Mechanism and Machine Theory*, vol. 76, pp. 20–38, 2014.

[21] H. H. Lin, F. B. Oswald, and D. P. Townsend, "Dynamic loading of spur gears with linear or parabolic tooth profile modifications," *Mechanism and Machine Theory*, vol. 29, no. 8, pp. 1115–1129, 1994.

[22] G. Bonori, M. Barbieri, and F. Pellicano, "Optimum profile modifications of spur gears by means of genetic algorithms," *Journal of Sound and Vibration*, vol. 313, no. 3–5, pp. 603–616, 2008.

[23] G. Liu and R. G. Parker, "Dynamic modeling and analysis of tooth profile modification for multimesh gear vibration," *Journal of Mechanical Design*, vol. 130, no. 12, 2008.

[24] S. S. Ghosh and G. Chakraborty, "On optimal tooth profile modification for reduction of vibration and noise in spur gear pairs," *Mechanism and Machine Theory*, vol. 105, pp. 145–163, 2016.

[25] H. Ma, X. Pang, R. Feng, and B. Wen, "Evaluation of optimum profile modification curves of profile shifted spur gears based on vibration responses," *Mechanical Systems and Signal Processing*, vol. 70-71, pp. 1131–1149, 2016.

[26] Z. Hu, J. Tang, J. Zhong, S. Chen, and H. Yan, "Effects of tooth profile modification on dynamic responses of a high speed gear-rotor-bearing system," *Mechanical Systems and Signal Processing*, vol. 76-77, pp. 294–318, 2016.

[27] V. Abousleiman and P. Velex, "A hybrid 3D finite element/lumped parameter model for quasi-static and dynamic analyses of planetary/epicyclic gear sets," *Mechanism and Machine Theory*, vol. 41, no. 6, pp. 725–748, 2006.

[28] C.-J. Bahk and R. G. Parker, "Analytical investigation of tooth profile modification effects on planetary gear dynamics," *Mechanism and Machine Theory*, vol. 70, pp. 298–319, 2013.

[29] H. H. Lin, D. P. Townsend, and F. B. Oswald, "Profile Modification to Minimize Spur Gear Dynamic loading," NASA Technical Memorandum 89901, American Society of Mechanical Engineers, Orlando, FL, USA, 1988.

[30] H. H. Lin, J. Wang, F. B. Oswald, and J. J. Coy, "Effect of extended tooth contact on the modeling of spur gear transmissions," *Gear Technology*, vol. 11, pp. 18–25, 1994.

[31] Z. Chen and Y. Shao, "Dynamic features of planetary gear train with tooth errors," *Proceedings of the Institution of Mechanical Engineers, Part C: Journal of Mechanical Engineering Science*, vol. 229, no. 10, pp. 1769–1781, 2015.

[32] J. Lin and R. G. Parker, "Analytical characterization of the unique properties of planetary gear free vibration," *Journal of Vibration and Acoustics*, vol. 121, no. 3, pp. 316–321, 1999.

[33] M. Inalpolat and A. Kahraman, "A theoretical and experimental investigation of modulation sidebands of planetary gear sets," *Journal of Sound and Vibration*, vol. 323, no. 3–5, pp. 677–696, 2009.

[34] V. Abousleiman, P. Velex, and S. Becquerelle, "Modeling of spur and helical gear planetary drives with flexible ring gears and planet carriers," *Journal of Mechanical Design*, vol. 129, no. 1, pp. 95–106, 2007.

[35] M. Chapron, P. Velex, J. Bruyère, and S. Becquerelle, "Optimization of profile modifications with regard to dynamic tooth loads in single and double-helical planetary gears with flexible ring-gears," *Journal of Mechanical Design*, vol. 138, no. 2, p. 023301, 2015.

[36] P. Dong, Y. Liu, P. Tenberge, and X. Xu, "Design and analysis of a novel multi-speed automatic transmission with four degrees-of-freedom," *Mechanism and Machine Theory*, vol. 108, pp. 83–96, 2017.